الجمـــهوريـــة الجـــزائريـــة الديـمقـراطيـــــــة الشـــعبيـــــة
PEOPLE'S DEMOCRATIC REPUBLIC OF ALGERIA
وزارة التعـلـيـم الـعـالـــي والـبـحـث الـعـلـمي
MINISTRY OF HIGHER EDUCATION AND SCIENTIFIC RESEARCH
جـامـعـة عمّـــار ثـلـيـــجـــي بالأغـــواط
UNIVERSITY AMAR TELIDJI LAGHOUAT
كـلـيـــــة الـعـلـــــوم
FACULTY OF SCIENCES
قسم عـلـــــوم المادة
Department Of Material Sciences

Master thesis

Domain : Material Sciences
Field : Physics
Option : Material physics

by:
HADBI Mohammed

THEME

Theoretical study of structural, electronic and mechanical properties of the ternary polar intermetallic compounds A_2MSb (A=Na, K and M=Au, Ag)

Publicly defended before the jury consisting of:

Mr. LAGOUNE Brahim	M.C.A	*President*
Mr. BOUCHENAFA Mohamed	M.A.A	*Examiner*
Mr. CHERIET Abderrahmane	M.A.A	*Examiner*
Mr. MAABED Said	M.A.A	*Supervisor*
Mr.KHAMELOUL Fakhereddine		*Co-supervisor*

2017- 2018

Dedication

Dedicate this work to my precious parents, and my family
Dedicate to all my wonderful teachers and professors
Dedicate to all my friends
Dedicate to …

ACKNOWLEDGEMENTS

First thanks are to Allah, we praise him and to inspire the patients in this research.

First of all, I want to thank my supervisor Mr ***MAABED SAID***

assistant professor -A- at the university Ammar Thelidji of Laghouat, and Mr ***KHAMLOUL Fakherddine,*** *for their*

sympathy, encouragement, help and dedication to the work.

My thanks also go to Mr ***LAGHOUN Brahim****, Mr* ***BOUCHENAFA Mohammed*** *and* ***CHERIET Abdelrahmane*** *for the interest*

which 'they brought to my initiation to research by agreeing to examine this work and enrich it with their proposals.

I would also like to thank all the teachers, and a special mention of

Mr LEFKAIER Ibn Khaldoun, Mr HELIFA Bachir , BELACEL Amar, BENTRIA Bachir and Mr HALIT Mohamed …

List of Figures

Chapter I: Bibliographic review

Chapter II: Theoretical background

Chapter III: Results and discussion

List of Tables

Bibliographic review

Chapter II: Technical computational

Chapter III: Results and discussion

Table of Contents

Chapter III: Results and discussion

Introduction

Introduction

To understand what happens to matter at the atomic level, or to discover new materials, scientific researchers resort using to experiments, computer simulations and then obtaining the results, through which we identify their physical properties (structural, mechanical, electronic and optical… etc). In this work, we tried to study physical properties of the ternary polar intermetallic compounds Na_2AuSb, *Na2AgSb* and K_2AuSb. Usually, polar intermetallic compounds are produced by a reaction between an electropositive element of group 1 (an alkaline) or of group 2 (an alkaline earth metal) with an electronegative element (transition metal or element of groups 13, 14, 15 or 16)[1].

To gain knowledge on the physical properties of the ternary alkali metal antimonides A_2MP (*A=Na, K* and *M=Cu, Ag*), first principles calculations have been performed. Density functional theory (DFT) calculations allow the prediction and calculation of material behavior based on quantum mechanical considerations, without requiring higher order parameters such as fundamental material properties. In the contemporary DFT technical, the electronic structure and the subsequent physical properties are evaluated using a potential acting on the system's electrons. Based on the pseudopotential plane wave (PP-PW) approach of density functional theory[2], the present investigation is aimed to report on the hitherto unexplored physical properties of the ternary orthorhombic alkali metal antimonides A_2MP (*A=Na, K* and *M=Cu, Ag*). Particular attention is paid to investigate their structural, elastic and electronic properties. The semilocal GGA-PBE functional was applied to describing all the aforementioned properties[3].

The remainder of this document is divided into three chapters. The first chapter is a review of the bibliography on the Zintl phases and the herein considered polar intermetallic compounds. The second chapter describes the theoretical framework in which this study was conducted. We present in this chapter the fundamentals of the density functional theory (DFT) and the approximations used to solve the Kohn-Sham mono-electronic equations, and give a short review on the mechanical properties of crystals. The third chapter present the results and interpreting obtained using methods reviewed in the second chapter.

References

[1] S.C. Sevov, Zintl phases, Intermetallic Compounds-Principles and Practice: Progress, Volume 3 (2002) 113-132.

[2] J.P. Perdew, Unified theory of exchange and correlation beyond the local density approximation, Electronic structure of solids' 91 11 (1991).

[3] J.P. Perdew, K. Burke, M. Ernzerhof, Generalized gradient approximation made simple, Physical review letters 77 (1996) 3865.

Chapter I
Bibliographic review

Chapter I: Bibliographic review

I.1 Introduction

Firstly, in this chapter, we give a short definition about Zintl Phases, and then we provide a review on the ternary polar intermetallic compounds (*Na_2AuSb, Na2AgSb, K_2AuSb*).

I.2 The zintel phases

Zintl phases are those compounds composed of electropositive metals (e.g. alkali metals, alkaline earth metals, and rare earth metals) and electronegative metals around the "zintl line", which divides columns 13 and 14 in the periodic table. Polar intermetallic phases have the definition similar to zintl phases but, in general, the electronegativity difference ($\Delta\chi$) between the constituting electropositive and electronegative metals is smaller than in zintl phases. However, there is no specific critical $\Delta\chi$ that separates zintl phases and polar intermetallic compounds [1].

Zintl phases are defined as follows. They are compounds that:

- Contain an alkali or alkaline-earth metal and element (or elements) that is a metal, semimetal, or small-gap semiconductor.
- Are electronically balanced or closed-shell compounds, i.e. the number of electrons provided by the constituting elements equals the number of electrons needed for covalent bonding in the structure.
- Have very narrow or no homogeneity width, i.e. they are line compounds.
- Are semiconductors or poor conductors.
- Are diamagnetic or show very weak, temperature independent paramagnetic.
- Are brittle.

The Zintl concept provides a simple idea about ionic and covalent bonding in intermetallic phases, allowing a simple description of the bond that gives an overview of the structure and properties of the intermetallic phases [2].

I.3 Ternary alkali metal A_2MP (A=Na, K and M=Cu, Ag)

I.3.1 Historical

In 1977, Gerhard Sayelsberg and *al.* published a paper titled 'preparation and crystal structure of *Na_2CuP, K_2AgAs, K_2AgSb*, and *K_2AgBi*', in this work, the orthorhombic structure type of *Na_2AgSb* (space groupe Cmcm (N=°63)) has been assigned to these to these compounds [3]. After a year,

another research group has published a new paper in which Na_2AgSb was found to crystallize in the same orthorhombic structure. The structure contains zigzag-chains with angle *Sb-Ag-Sb = 64.9°* [4]. Two years later, three new compounds Na_2AuAs, Na_2AuSb, K_2AuSb were prepared [5], these compounds where found to crystalize in Na_2AgSb type structure. Results from this work are summarized in table *I-1*:

TableI.1: *lattice parameters of Na_2AuSb and K_2AuSb compounds.*

Crystal system orthorhombic	Na_2AuSb	K_2AuSb
lattice constants [pm]	$a = 927,9$	$a = 1045,9$
	$b = 756,2$	$b = 786,1$
	$C = 584.1$	$C = 650.0$
Density [g/cm^3]	5.90	5.01

In 2009 , A_2AuBi (*A*=Na, K) and K_2AuSb were obtained by direct reaction of the elements at elevated temperatures in niobium ampoules [6]. The three isotypic compounds extend the prominent A_2MPn (*M*= transition metal; *Pn* group 15) structure family. Single-crystal X-ray diffraction experiments show that these phases crystallize in the orthorhombic space group *Cmcm* (N^o: 63) with four formula units per one unit cell and (Z=4). The simple structures, which contain zigzag chains of linear two-bonded gold atoms and acute angles (64 to 76°) at two-bonded antimony or bismuth, can readily be rationalized with the Zintl-Klemm concept. TB-LMTO (The linear muffin-tin orbital)[7] calculations show distinct band gaps at E_F, and analyses of DOS and COHP (Crystal Orbital Hamilton Population)[8] curves show optimized *Au–Pn* bonding, appreciable *Au–Au* interactions across the chains, and covalent interactions between *A* and *Pn* atoms. The same structural motif exists for other phases containing group 11–12 metals, which also crystallize in orthorhombic space groups (see TableI-1**)**. All contain planar zigzag chains; however, in a few cases slight deviations from special positions and planarity (in Cmcm) are present.

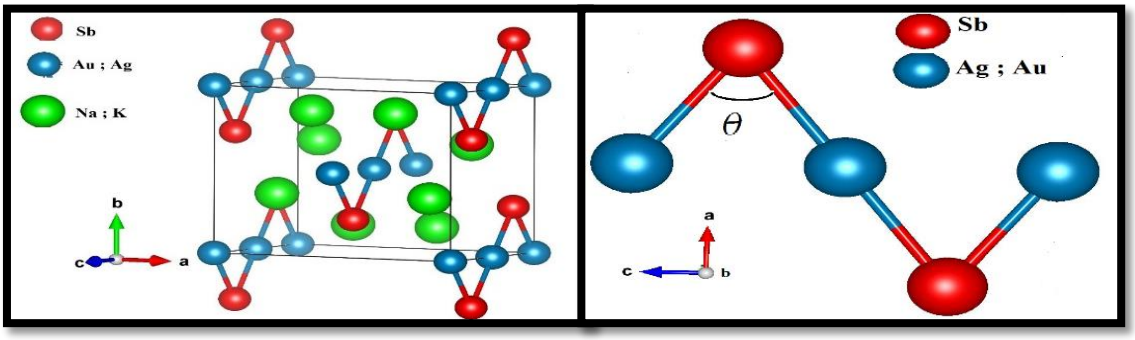

Figure I.1*: The Orthorhombic Structure (Cmcm) and angle zigzag chain of K_2AuSb, Na_2AuSb and Na_2AgSb.*

Table I.2: *Overview of Intermetallic A2MPn (A = Na, K; M = Cu–Au; Pn = As–Bi) and Cd/Pb Compounds, Bond lengths /Å, and Bond Angles /° at the p Block Element.*

A_2MPn	Space group (N°)	d_{M-M}	d_{M-Pn}	∠M–Pn–M
Na_2AuAs	*Cmcm (63)*	2.88	2.50	70
Na_2AuSb	*Cmcm (63)*	2.92	2.65	67
Na_2AuBi	*Cmcm (63)*	2.92	2.75	64
K_2AuSb	*Cmcm (63)*	3.25	2.64	76
K_2AuBi	*Cmcm (63)*	3.30	2.73	74
Na_2AgAs	$C222_1$ (20)	2.80	2.52	68
Na_2AgSb	Cmcm (63)	2.89	2.69	65
K_2AgAs	$C222_1$ (20)	3.01	2.54	73
K_2AgBi	$C222_1$ (20)	3.17	2.76	70
Na_2CuAs	Cmcm (63)	2.67	2.34	70
K_2CuAs	*Cmcm (63)*	2.95	2.33	78
K_2CuSb	*Cmcm (63)*	3.12	2.51	77
K_2CdPb	*Ama*2 (40)	3.23	2.84	69

I.4 Crystal structure of Na_2AuSb, Na_2AgSb and K_2AuSb

Under normal conditions, the considered compounds adopt the orthorhombic *Na_2CuAs*-type structure (space group Cmcm, No.63), with four formula units (i.e *Na2AgSb*) per one unit cell (Z=4). Figure. I.1 depicts a prototype conventional cell, which is built according to the experimental data from Refs [4]. The structure feature one-dimensional infinite poly-anionic units forming zigzag chains along the c-axis [6]. The antimony atoms at 4c Wyckoff sites in the zigzag chains are distributed alternatively up and down around the transition metal atoms (4b sites). The angles in the chains occur at the antimony atoms, which are linearly coordinated by their adjacent transition metal atoms. The chains are juxtaposed in the (bc) planes forming antimony /transition metal slabs separated by puckered layers of alkali metal cations at 8g sites along the a-axis [3]. The stacking arrangement of the alkali metal layers creates large channels along the c-axis enfolding the zigzag chains.

I.5 Applications of Zintl phases for thermoelectric devices

By converting waste heat into electricity and improving the efficiency of refrigeration systems, thermoelectric devices could play a significant role in solving today's energy problems. Increasing the thermoelectric efficiency (as measured by the thermoelectric material's figure-of-merit, ZT) is critical to the development of this technology. Complex Zintl phases, in particular, make ideal candidates for thermoelectric materials because the necessary "electron–crystal, phonon–glass" properties can be engineered with an understanding of the Zintl chemistry. A transition metal Zintl compound, has twice the ZT as the material currently in use at NASA. This perspective outlines a strategy to discover new high zT materials in Zintl phases, and presents results pointing towards the success of this approach [9].

References

[1] F. Wang, Rationalizing the structures of Zintl and polar intermetallic phases, Iowa State University2011.

[2] S.C. Sevov, Zintl phases, Intermetallic Compounds-Principles and Practice: Progress, Volume 3 (2002) 113-132.

[3] G. Savelsberg, H. Schäfer, Darstellung und Kristallstruktur von Na2CuP, K2AgAs, K2AgSb und K2AgBi/Preparation and Crystal Structure of Na2CuP, K2AgAs, K2AgSb, and K2AgBi, Zeitschrift für Naturforschung B 32 (1977) 745-748.

[4] H. Schuster, C. Mues, W. Jung, Darstellung und Kristallstruktur des Na2AgSb, Z. Naturforsch. 34b (1979) 354-355.

[5] C. Mues, H.-U. Schuster, Na2AuAs, Na2AuSb, K2AuSb-drei neue A2BX-Verbindungen mit BX-Kettenstruktur/Na2AuAs, Na2AuSb, K2AuSb-Three New A2BX Compounds with a BX Chain Structure, Zeitschrift für Naturforschung B 35 (1980) 1055-1058.

[6] S.J. Kim, G.J. Miller, J.D. Corbett, Zigzag chains of alternating atoms in A2AuBi (A= Na, K) and K2AuSb. Synthesis, structure, and bonding, Zeitschrift für anorganische und allgemeine Chemie 636 (2010) 67-73.

[7] J.M.W.a.A.A.D.E. Grechnyev, Linear Muffin-Tin Orbital Method in the Atomic Sphere Approximation, (2010).

[8] V.L. Deringer, A.L. Tchougréeff, R. Dronskowski, Crystal Orbital Hamilton Population (COHP) Analysis As Projected from Plane-Wave Basis Sets, The Journal of Physical Chemistry A 115 (2011) 5461-5466.

[9] S.M. Kauzlarich, S.R. Brown, G.J. Snyder, Zintl phases for thermoelectric devices, Dalton Transactions (2007) 2099-2107.

Chapter II

Theoretical background

Chapter II: Theoretical background

I.1 Introduction

In solid, the interactions between their electrons determine most of its physical properties; this brings us to a study of these interactions in order to understand the relationship between most of these physical properties. Then we can theoretically predict these properties without resorting to experience.

In 1926, Erwin Schrödinger wrote an equation describing the movement of the electron and the possibility of its presence in a limited area. The application and resolution of this equation on a solid can give us an idea of its physical properties (electrical, optical and mechanical).

I.2 The Schrödinger equation

For a solid body consisting of N cores and n_e electrons. The generalized Schrödinger equation is writing as follows:

$$H\Psi(\vec{R},\vec{r},t) = E\Psi(\vec{R},\vec{r},t) \qquad \text{(II.1)}$$

Where ***H*** is the Hamiltonian of the system given by the following relation**:**

$$H = T_N + T_e + U_{ee} + U_{Ne} + U_{NN} \qquad \text{(II.2)}$$

Whereas**:**

- $T_N = -\sum_I^N \frac{\hbar^2}{2M_I}\nabla_I^2$: The kinetic energy of the nuclei.
- $T_e = -\sum_i^n \frac{\hbar^2}{2m_e}\nabla_i^2$: The kinetic energy of electrons.
- $U_{ee} = \sum_{i=1}^n \sum_{j>i}^n \frac{e^2}{4\pi\varepsilon_o}\frac{1}{\left|\vec{r}_i - \vec{r}_j\right|}$: The interaction energy between electrons.
- $U_{Ne} = \sum_{i=1}^n \sum_{I=1}^N \frac{e^2}{4\pi\varepsilon_o}\frac{Z_I}{\left|\vec{r}_i - \vec{R}_I\right|}$: The potential energy of the Coulomb attraction between electrons and nuclei.

- $U_{NN} = \sum_{I=1}^{N}\sum_{J>i}^{N} \frac{e^2}{4\pi\varepsilon_o} \frac{Z_I Z_J}{\left|\vec{R}_I - \vec{R}_J\right|}$: The potential energy due to repulsion between nuclei.

- E : The value clean of the Hamiltonian, it represents the total energy of the system.

- $\Psi(\vec{R},\vec{r},t)$: Represent the wave function of all coordinates (R_I nuclei position $I = 1, \ldots, N$. And r_i is electrons position $i = 1, \ldots, n$; t is time) of the all nuclei and electrons of the system.

In order to simplify the equation we use atomic units the following table summarizes these units:

Table II.1: *Atomic unit used in DFT and their equivalents in the international system (SI).*

Sizes	Symbols	SI Unit	Atomic unit (*u.a*)
Electron mass	m_e	$9.1096 \cdot 10^{-31} kg$	$1\ u.a$
Charge of the electron	e	$-1.6022 \cdot 10^{-19} C$	$1\ u.a$
Reduced Planck constant	$\hbar$	$1.0646 \cdot 10^{-34} J.s$	$1\ u.a$
Length (the Bohr radius)	$a_0 = \frac{4\pi\varepsilon_0\hbar}{m_e e^2}$	$0.52918 \cdot 10^{-10} m$	$1\ u.a = 1\ Bohr$
Energy (Hartree)	$E_0 = \frac{\hbar^2}{m_e a_0^2}$	$4.3598 \cdot 10^{-18} J$	$1\ u.a = 1\ Hartree$

After using this units we can write Schrödinger equation in the form:

$$\left[-\sum_{i}^{n}\frac{1}{2}\nabla_i^2 - \sum_{I}^{N}\frac{1}{2M_I}\nabla_I^2 + \sum_{I=1}^{N}\sum_{J>I}^{N}\frac{Z_I Z_J}{\left|R_I - R_J\right|} + \sum_{i=1}^{n}\sum_{j>i}^{n}\frac{1}{\left|\vec{r}_i - \vec{r}_j\right|} - \sum_{i=1}^{n}\sum_{I=1}^{N}\frac{Z_I}{\left|\vec{r}_i - \vec{R}_I\right|}\right]\Psi(\vec{R}_I,\vec{r}_i) = E\Psi(\vec{R}_I,\vec{r}_i)$$

(II.3)

Solving of this equation it's very difficult in the case of multiple particles. In this state Physicists have developed approximate methods to solve this equation.

I.3 The Born-Oppenheimer Approximation

Is to decouple the movement electrons from that of the nuclei. Indeed the ratio between the mass of the electron and the mass of any atomic nucleus is very weak. So the electrons move so much faster than atomic nuclei. In this approximation, the electrons are always in their fundamental

state, whatever the position of the atomic nuclei. The problem therefore goes from a system of $N_e + N_n$ interacting particles to a N_e system. Electrons interacting in an external potential generated by the nuclei. The positions of atomic nuclei are just parameters in solving the problem. The interaction term between the nuclei only intervenes in the calculation of the total energy of the system, but not in the calculation of the electronic wave functions. The Hamiltonian reduced to its only electronic components therefore written:

$$H_e = T_e + U_{ee} + U_{Ne} \tag{II.4}$$

We can write a Schrödinger equation on electrons:

$$H_e \psi_e = E_e \psi_e \tag{II.5}$$

The wave function of system as a product of two wave functions:

$$\Psi\left[\left\{\vec{R_I}\right\},\left\{\vec{r_i}\right\}\right] = \psi_e\left[\left\{\vec{R}_I\right\},\left\{\vec{r}_i\right\}\right] \times \varphi_N\left[\left\{\vec{R}_I\right\}\right] \tag{II.6}$$

This approximation not give real energy, so physicists developed other approach methods for giving more accurate.

I.4 Hartree and Hartree-Fock approximation

The Hartree-Fock method is a method of approximate resolution of the Schrödinger equation of a multi-body quantum system using the variational principle to approximate the wave function and the energy of the fundamental level stationary. The method usually assumes that the wave function of the multi-body system can be roughly written as a Slater determinant when the particles are fermions, or as a permanent for the case of bosons.

The idea is to assume that the electrons move independently of each other. That is to say that the probability of finding the coordinate electron r_1 in the orbital 1 is independent of that of other electrons. Then the electronic wave function can be written as a product of electronic mono waves:

$$\psi_e\left[\left\{\vec{r}_e\right\},\left\{\vec{R}_I\right\}\right] = \psi_1(\vec{r}_1).\psi_2(\vec{r}_2).....\psi_{Ne}(\vec{r}_{Ne}) \tag{II.7}$$

Therefore, can be write Schrödinger equation in form:

$$H_H \psi_i(\vec{r}_i) = \varepsilon_i \psi_i(\vec{r}_i) \tag{II.8}$$

And

$$H_H = -\frac{1}{2}\nabla_i^2 + U_{ext}(\vec{r},\vec{R}) + U_H(\vec{r}) \qquad \text{(II.9)}$$

Where:

- $U_{ext}(r,R)$: the potential to the electron-nuclei interactions and those of other electrons, nuclei.
- U_H : the potential of Hartree associated with Coulomb interaction with other electrons.

Hartree-Fock suggested that the wave function is a slater-determinate form:

$$\psi_e = \psi_{DS} = \frac{1}{\sqrt{N!}}\begin{vmatrix} \psi_1(\vec{r}_1) & \psi_2(\vec{r}_1) & \cdots & \psi_N(\vec{r}_1) \\ \psi_1(\vec{r}_2) & \psi_2(\vec{r}_2) & \cdots & \psi_N(\vec{r}_2) \\ \vdots & \vdots & \ddots & \vdots \\ \psi_1(\vec{r}_N) & \psi_2(\vec{r}_N) & \ldots & \psi_N(\vec{r}_N) \end{vmatrix} \qquad \text{(II.10)}$$

The exchange of two particles is equivalent to the exchange of two columns, which produces, due to a known property of determinants, a change of sign. Note that if two rows are equal, the determinant is zero: all ψ_i must be deferent. This demonstrates Pauli's exclusion principle: two (or more) identical fermions cannot occupy the same state.

(ψ_i Composed two part: orbital function and spatial function, and $\frac{1}{\sqrt{N!}}$: normalization factor**).**

After simplify the Hamiltonian H_H find:

$$\left(-\frac{1}{2}\nabla_i^2 + U_{ext}(\vec{r},\vec{R}) + \sum_{\substack{j=1 \\ j\neq i}}^{n}\int\frac{\left|\varphi_j(\vec{r'})\right|^2}{\left|\vec{r}-\vec{r'}\right|}d\vec{r'}\right)\varphi_i(\vec{r}) - \sum_{\substack{j=1 \\ j\neq i}}^{n}\int\frac{\varphi_j(\vec{r})\varphi_j^*(\vec{r'})}{\left|\vec{r}-\vec{r'}\right|}d\vec{r'}\varphi_i(\vec{r'}) = \varepsilon_i\varphi_i(\vec{r}_i) \qquad \text{(II.11)}$$

Where:

$-\frac{1}{2}\nabla_i^2$: The kinetic energy of the electron i.

$U_{ext}(\vec{r},\vec{R})$: The energy of attraction between nuclei and electrons

$\sum_{\substack{j=1 \\ j\neq i}}^{n} \int \frac{\left|\varphi_j(\vec{r'})\right|^2}{\left|\vec{r}-\vec{r'}\right|} dr'$: The integral of Coulomb noted (the potential of Hartree).

$\sum_{\substack{j=1 \\ j\neq i}}^{n} \int \frac{\varphi_j(\vec{r})\varphi_j^*(\vec{r'})}{\left|\vec{r}-\vec{r'}\right|} dr'$: The exchange integral.

I.5 Density functional theory (DFT)

All the precedents approximations based on electronic wave function. Therefore, the calculation and resolution Schrodinger equation is very difficulte. One of the most used ab-initio methods is the theory of the functional of the density (DFT**)** is a reformulation of the quantum N body problem into an electronic density problem only .

Thomas and Fermi (1927,1928), are the first to have a theory that goes in this direction, but it has proved defective many points. Later, Hohenberg, Kohn and Sham have taken up this idea and proposed a more elaborate theory that allows to better account for kinetic energy and exchange and correlation energy.

I.5.1 Thomas –Fermi model

The **Thomas–Fermi** (**TF**) **model** [1, 2] named after Llewellyn Thomas and Enrico Fermi, is a quantum mechanical theory for the electronic structure of many-body systems developed semiclassically shortly after the introduction of the Schrödinger equation [3] It stands separate from wave function theory as being formulated in terms of the electronic density alone and as such is viewed as a precursor to modern density functional theory. The TF model is correct only in the limit of an infinite nuclear charge. Using the approximation for realistic systems yields poor quantitative predictions, even failing to reproduce some general features of the density such as shell structure in atoms and Friedel oscillations in solids. It has, however, found modern applications in many fields through the ability to extract qualitative trends analytically and with the ease at which the model can be solved. The kinetic energy expression of Thomas–Fermi theory is also used as a component in more sophisticated density approximation to the kinetic energy within modern orbital-free density functional theory.

Working independently, Thomas and Fermi used a statistical model in 1927 to approximate the distribution of electrons in an atom. Although electrons are distributed nonuniformly in an atom, an approximation was made that the electrons are distributed uniformly in each small volume

element ΔV (i.e. locally) but the electron density $n(\vec{r})$ can still vary from one small volume element to the next.

$$E_0 = [n] \tag{II.12}$$

$$T_{TF} = [n] = \int t\left[n(\vec{r}) \right] dr \tag{II.13}$$

$$\boldsymbol{t}\left[\boldsymbol{n}(\vec{\boldsymbol{r}}) \right] = \frac{3}{5} n(\vec{r}) E_F \tag{II.14}$$

$$E[\vec{\psi}] = E[n] = T[n] + U_{ee}[n] + \int U_{ext}(\vec{r}) n(\vec{r}) dr \tag{II.15}$$

$\boldsymbol{t}\left[\boldsymbol{n}(\boldsymbol{r}) \right]$: represent the kinetic energy density of electrons system without interaction.

If the electronic density of a system whatever is given, this functional allows to calculate explicitly the total energy, which we obtain the minimization of the functional over all possible densities.

I.5.2 Hohenberg-Kohn theorems

First Theorem:

« For any system of interacting particles in an external potential $U_{ext}(\vec{r})$**,** the density is uniquely determined (in other words, the external potential is a unique functional of the density) » [4].

Which is clearly a contradiction. Thus the theorem has been proven by evidence absurd.

Second Theorems:

The energy reaches the minimum real density (the electronic density of the system in the ground state is that the total energy is reduced to a minimum) [4].

$$E\left[n_0(t) \right] \leq E\left[n(t) \right] \tag{II.16}$$

I.5.3 Kohn-Sham equations

Kohn and Sham propose to replace multi particle systems in interaction by a system without interaction easier to solve. Approach Kohn and sham assumed that the electron density in the ground state of the real system is equal to that of other fictitious system particles without

interaction. This leads to solving a set of equations for independent particles like those of Hartree or Hartree-fock:

$$H_{KS}\varphi_i(\vec{r}) = \varepsilon_i\varphi_i(\vec{r}) \tag{II.17}$$

With:

$$H_{KS} = -\frac{1}{2}\nabla_i^2 + U_{eff}(\vec{r}) \tag{II.18}$$

And:

$$U_{eff} = U_{ext}(\vec{r}) + \int \frac{n(\vec{r}')}{|\vec{r} - \vec{r}'|} dr' + U_{xc}(\vec{r}) \tag{II.19}$$

The problem is that we cannot define the term of exchange and correlation of exact handling. So we must make approximations.

I.5.4 Local density approximation (LDA)

Assume that the density of a particulate in point r, does not depend only on the density in r, and that it is equal to the correlation energy per particle of a homogeneous gas of density $n(r)$:

$$E_{xc}^{LDA}\left[n(\vec{r})\right] = \int n(\vec{r})\varepsilon_{xc}^{LDA}(n(\vec{r}))dr \tag{II.20}$$

Or the exchange energy -correlation can be decomposed as the sum of the exchange energy and the correlation energy.

$$\varepsilon_{xc}^{LDA}\left[n(\vec{r})\right] = \varepsilon_x\left[n(\vec{r})\right] + \varepsilon_c\left[n(\vec{r})\right] \tag{II.21}$$

The term exchange energy is known giving by functional energy exchange of Thomas- Fermi-Dirac:

$$\varepsilon_x^{LDA}(\vec{r}) = -\frac{3}{4}\left(\frac{3}{\pi}\right)^{\frac{1}{3}} n(\vec{r})^{\frac{1}{3}} \tag{II.22}$$

On the other hand, the correlation energy, which is more complex to evaluate, to evaluate we use quantum Carlo-methodes [5].

I.5.5 Generalized Gradient Approximation (GGA)

The LDA approach is based on the homogeneous electrons gas model, and therefore assumes a uniform electron density. However, atomic or molecular systems are most often very different from a homogeneous electron gas, in a more general way, we can consider that all real systems are inhomogeneous, which means the electronic density has a spatial variation (locale). Most of the corrections that have been introduced at the LDA are based on the idea of taking into account local variations in density.

For this reason, the gradient of the electronic density has been introduced leading to the approximation of the generalized gradient (GGA, generalized Gradient Approximations), in which the exchange energy and correlation is depending on the electron density and its gradient. In which the exchange energy and correlation is depending on the electron density and its gradient:

$$E_{xc}^{GGA}\left[n(\vec{r}),\nabla n(\vec{r})\right]=\int n(\vec{r})\varepsilon_{xc}^{GGA}\left[n(\vec{r}),\nabla n(\vec{r})\right]dr \qquad \text{(II.23)}$$

There are many expressions to describe the GGA functional following the choice of $\varepsilon_{xc}\left[n(r),\nabla n(r)\right]$ as forms of Becke (B88) [6]. from Perdew-Wang (PW91) [7] and Perdew-Burke-Ernzerhof (PBE) [8] Hansen and Norskov (RPBE) [9].

I.5.6 Hybrid Functional

Use of the LDA or the GGA under the DFT allows a description surprisingly accurate most of the properties of solids and molecules. However, the use of these two approximations still generates some significant errors especially when calculating the fundamental energy of small molecules and the gap extended systems.

In order to compensate for these flaws, a new generation of functionalities has been recently developed. In these models, the exchange-correlation energy functional makes both Hartree-Fock and other formalism of the DFT (LDA or GGA), hence their name of functional hybrids. Currently, the most common hybrid functional are PBE0, HSE03, HSE06 and B3LYP [10]. The use of such functionalities makes it possible to get closer to the data known experimental, such as lattice parameters, or the energy gap some systems.

In general, hybrid functionalities are particularly effective for the description of molecules and insulating materials, semiconductors and transition metal oxides. Their major disadvantage is

that such calculations are generally greedy in computing resources than for conventional functional, because of the incorporation of terms Hartree-Fock.

I.6 Calculation methods

I.6.1 Pseudopotential method

The pseudo-potential approach is based on the assumption that most of the properties physical systems electronic systems are much more dependent on valence electrons than of the heart electrons, the bonding of the atoms is essentially due to the valence electrons while heart electrons can be considered frozen and so they can to be ignored in most cases.

***Figure II.1**: Comparison of a wave function in the coulomb potentiel of the nucleu to the one in the pseudopotentiel .the real and the pseudo wave function and potential match above a certain cutoff radius*

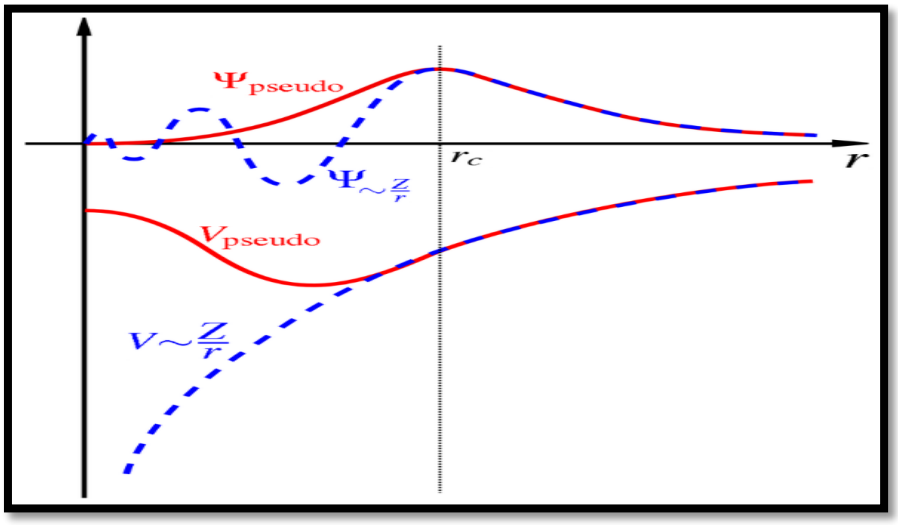

r_c .

Practically, pseudo potentials are constructed so that beyond a certain ray of *Cut-off* $\boldsymbol{r_c}$, defining a sphere inside which the electrons are located of heart, the pseudo potential and the valence wave pseudo-functions must be identical true potential and true valence wave functions [11].

I.6.2 Plans waves

Plane waves are exact the proper functions of a homogeneous electron gas system. This is the natural choice of the base in the case of simple metals [12]. Waves planes are orthonormal and independent of energy, so the Schrödinger equation transforms into a simple eigenvalue matrix

problem and since plane waves do not do not depend on the atomic positions, so we can apply the Hellman- Feynman directly to calculate the forces acting on the atoms. On the other hand, convergence is simple, since increasing the number of waves increases accuracy. The choice of number of plane waves to use is truncated by a so-called cutoff energy $\boldsymbol{E_{cut}}$ such as:

$$\frac{1}{2}\left|K+G\right|^2 \leq E_{cut} \qquad \text{(II.24)}$$

For determine this very important calculation parameter one must always make a convergence study.

I.7 Technical Calculation

I.7.1 Periodic Systems and Bloch theorem

Bloch theorem is a consequence of the periodicity of the crystalline potential; it illustrates the invariance of the system by translational symmetry. The wave function is then written as the product of a periodic function, $\boldsymbol{U_j^k}$ clean lattice , and a plane wave, which translates the lattice translation[13].

$$\psi_j^k(\vec{r}) = u_j^k(\vec{r})e^{i(\vec{k}.\vec{r})} \qquad \text{(II.25)}$$

$$u_j^k(\vec{r}) = \sum_G \tilde{u}(\vec{G})e^{i(\vec{G}.\vec{r})} \qquad \text{(II.26)}$$

The vectors $\vec{K}$ and $\vec{G}$ are defined in reciprocal space within the first zone Brillouin. the wave vector $\vec{K}$ is a quantum number own orbital Bloch. The solving Kohn and Sham equations within a periodic system is done necessarily for a finite number of points K obtained by representative sampling and suitable of the ZB that allows to reproduce faithfully its symmetry.

I.7.2 Sampling of the Brillouin Zone (BZ)

Brillouin-zone sampling in total-energy calculations of aperiodic systems using periodic boundary conditions is considered. Although the energies converge to the exact result in the limit of large supercells for any k-point sampling scheme, they do not converge at the same rate. In particular, shown that the use of a single sampling point at the origin of reciprocal space is

especially inefficient. A k-point sampling scheme is proposed, which is computationally efficient and its efficacy relative to other common approaches is demonstrated [14].

I.8 Calculation Code: CASTEP

All the calculations presented in the manuscript were made using a code of numerical modeling called CASTEP (Cambridge Serial Total Energy Package) [15]. This code was originally developed in 1988 by Payne et al [16]. This is a calculation code ab initio and it is part of a set of digital simulation software named Materials Studio (MS) and marketed by Dassault Systems Biovia©.

CASTEP is developed by Condensed Matter Theory Group at the University of Cambridge, UK, it's a program that uses the functional density theory (DFT) to simulate the properties of the solids, and can predict properties, including elastic constants, structural properties, energy band diagrams, electronic state densities, charge densities and optical properties as well as vibrational properties and Thermodynamic. This code is used to simulate the total energy by special integration of K-points in the first Brillouin zone with a plane wave base for expansion of wave functions and the summation in this area is performed on the wave vectors produced by the Monkhorst and Pack method [17]. CASTEP runs on Windows and Linux. A graphical interface that complies with Microsoft Windows standards, allows the user to interact with graphic templates 3D, configure calculations and analyze results through simple dialogs and familiar to any Windows user.

I.9 Elastic properties of the solid

In physics, elasticity is the property of a solid material to return to its original shape after being deformed. The elastic deformation is a reversible deformation. Solid material deforms. When forces are applying to it, an elastic material regains its original shape and size when these forces no longer exerted, up to a certain limit of the value of these forces.

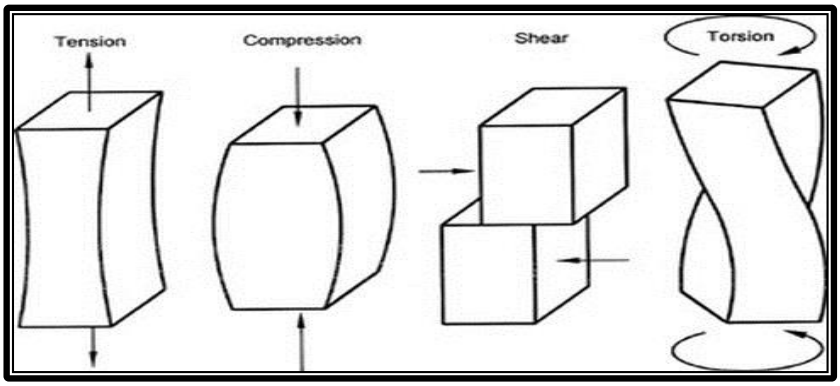

Figure II.2: *Elastic deformation of materials, we can subject the rigid bodies to 4 types of forces which cause deformations.*

I.9.1 Elastic constants

The limit elasticity of a material depends on several factors, the main ones being:

- Interatomic cohesion forces (bonds).
- The crystalline structure.
- The atoms strangers block dislocations (alloyed metals).
- Dislocations are blocked by grain boundaries.
- The dislocations are blocked between them.

Remind: The elastic limit also depends on the temperature.

I.9.2 Hook's Law

The relationship between deformation and stress in the elastic domain represented by Hook's law:

$$\sigma = E\varepsilon \tag{II.27}$$

E: The Young's modulus (rigidity) which characterizes the solid's resistance to uniaxial deformation. The Coefficient of compressibility $K\left[Pa\right]$ of the materials defined as:

$$B = -V_0 \frac{\Delta P}{\Delta V} = \frac{1}{3} \frac{E}{(1-2\upsilon)} \tag{II.28}$$

υ Poisson's coefficient of materials.

The relation between Young's modulus and Poisson's ratio:

$$G = \frac{1}{2} \frac{E}{(1+\upsilon)} \tag{II.29}$$

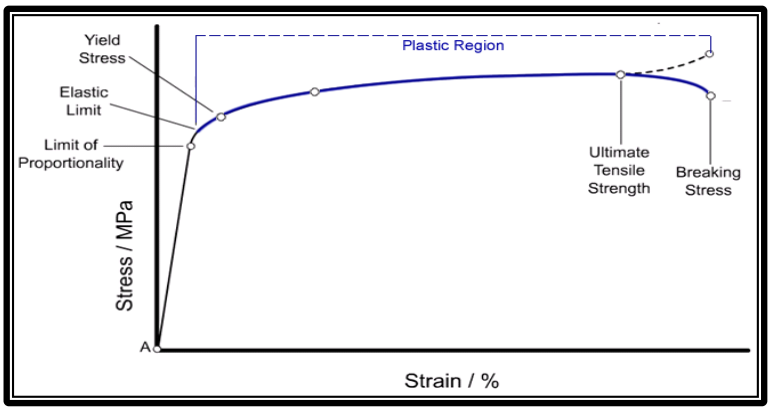

***Figure II.3**: Curve represent the range elastic of materials, the slope of this domain equivalent to Young's modulus.*

We can represent the constraint as a tensor $\boldsymbol{\sigma_{ij}}$ **,** as $\boldsymbol{i}$ indicates the direction of the force and $\boldsymbol{j}$ indicates the surface on which the force is applied, so we get 9 constrained, but thanks to the symmetry the number is reduced to 6. The same thing for the deformation, the tensor of deformations $\boldsymbol{\varepsilon_{ij}}$ contains 6 values, so according to Hooke's law, the relationship between constraint and strain is a matrix that contains 36 elements, it is the rigidity matrix:

$$\begin{pmatrix} \sigma_{11} \\ \sigma_{12} \\ \sigma_{13} \\ \sigma_{14} \\ \sigma_{15} \\ \sigma_{16} \end{pmatrix} = \begin{pmatrix} C_{11} & C_{12} & C_{13} & C_{14} & C_{15} & C_{16} \\ C_{21} & C_{22} & C_{23} & C_{24} & C_{25} & C_{26} \\ C_{31} & C_{32} & C_{33} & C_{34} & C_{35} & C_{36} \\ C_{41} & C_{42} & C_{43} & C_{44} & C_{45} & C_{46} \\ C_{51} & C_{52} & C_{53} & C_{54} & C_{55} & C_{56} \\ C_{61} & C_{62} & C_{63} & C_{64} & C_{65} & C_{66} \end{pmatrix} \begin{pmatrix} \varepsilon_{11} \\ \varepsilon_{12} \\ \varepsilon_{13} \\ \varepsilon_{14} \\ \varepsilon_{15} \\ \varepsilon_{16} \end{pmatrix} \qquad \text{(II.30)}$$

The variation of the potential energy of the low-deformation system is quadratic, which makes the matrix symmetrical with respect to the diagonal, the number of independent elastic constants thus becomes 21 instead of 36. This number also depends on the symmetry of the crystal lattice, allows reduced the stiffness constants. The number of C_{ij} remains 21 for the triclinic, because the last contains only one symmetry operation ($\bar{1}$), and becomes 3 for the cubic system because it contains 48 symmetry operations (the largest number of operations by contribution to the other systems). The number of elastic constants independent for the different crystal lattices is shown in the Table II-2. The inverse of the stiffness matrix is the flexibility matrix S_{ij} , which contains the same number of constants S_{ij} **.**

***Table II..2**: The number of C_{ij} for each crystal lattice.*

Crystal lattice	Number of C_{ij}
Triclinic	**21**
monoclinic	**13**
Orthorhombic	**9**
Tetragonal II (4,$\bar{4}$, $4/m$)	**7**
Tetragonal I (422, 4mm , 4/mmm)	**6**
Rhomboedric II (3,$\bar{3}$)	**7**
Rhomboedric I (32, 3m , $\bar{3}m$)	**6**
Hexagonal	**5**
Cubic	**3**

***Table II.3:** The physical meaning of each modulus of elasticity and the equation as a function of Cij (Voigt and Reuss methods).*

Moduli	Physical meaning	Equation
Compressibility	Resistance to volume change under hydrostatic pressure	$B_V = (C_{11}+C_{22}+C_{33}+2C_{12}+2C_{13}+2C_{23})/9$ $B_R = [(s_{11}+s_{22}+s_{33})+2(s_{12}+s_{23}+s_{31})]^{-1}$
Shear	Resistance to sliding motion of the planes inside the solid	$15G_V = (C_{11}+C_{22}+C_{33})-(C_{12}+C_{23}+C_{31})+3(C_{44}+C_{55}+C_{66})$ $15G_R = 4(s_{11}+s_{22}+s_{33})-4(s_{12}+s_{23}+s_{31})+3(s_{44}+s_{55}+s_{66})$
Young	Resistance to uni-axial deformation	$E = \frac{9BG}{3B+G}$
Poisson	Characterizes the traction and compression of the solid perpendicular to the direction of the force applied.	$\upsilon = \frac{3B+2G}{2(3B+G)}$

Modulus of elasticity (compressibility B, shear G, Young's modulus E and Poisson's ratio υ) are elastic quantities that describe the mechanical properties solid body. They are all expressed in terms of C_{ij} or S_{ij} **.** In the following paragraphs, we will take the orthorhombic system as an example because the materials we are studying crystallize in this structure (*Table II-3*). The modules of elasticity are calculated in three approaches, that of Voigt which gives the superior limit, that of Reuss which gives the lower limit and in the end the approach of Hill which is the average of the two.

I.9.3 Debye temperature and the elastic wave speed

One of the most important parameters that determines the thermodynamic properties materials (heat and melting temperature …) and the temperature of Debye θ_D**.** Generally, a high value of θ_D reveals a thermal conductivity and a melting high temperature. The temperature of Debye θ_D can be derived from isotropic acoustic wave velocities which are in turn connected to the isotropic modulus of elasticity [18].

$$\theta_D = \frac{h}{k_B}\left[\frac{3n}{4\pi}\left(\frac{N_A\rho}{M}\right)\right]^{1/3} v_m \qquad \text{(II.31)}$$

Where h is the Blanck constant, k_B is the Boltzmann constant, n is the number of atoms per molecule, N_A is the number of Avogadro, ρ is the density of material and M is the molecular mass. The average wave velocity of the sound v_m is given by the equation:

$$v_m = \left[\frac{1}{3}\left(\frac{2}{v_t^3} + \frac{1}{v_l^3}\right)\right]^{-1/3} \qquad \text{(II.32)}$$

In which v_t and v_l are respectively the acoustic wave velocities longitudinal and transverse. These two parameters can be estimated from the modules of compressibility B and shear G using the Navier equations [19].

$$v_l = \left(\frac{3B+4G}{3\rho}\right)^{1/2} \qquad \text{and} \qquad v_t = \left(\frac{G}{\rho}\right)^{1/2} \qquad \text{(II.33), (II.34)}$$

I.9.4 Elastic anisotropy

The elastic anisotropy represents the direction dependence of the elastic response of a material to external applied stress. It is defined by the universal anisotropy index that expresses itself according to the modules B_V , B_R , G_V and G_R as:

$$A^U = 5\frac{G_V}{G_R} + \frac{B_V}{B_R} - 6 \qquad \text{(II.35)}$$

A null value of A^U indicates a perfect isotropic behavior of the elastic properties marital, while a higher value indicates a certain degree of elastic anisotropy.

In an isotropic material, the Young's modulus and compressibility remain the same whatever the direction of the constraint. i.e, if we graphically present these modules in the form of a closed 3D surface as a function of the direction of the stress, we get a perfectly spherical shape. In this concept, every point of the surface is spotted by its position vector, whose amplitude gives a measure of the elastic modulus, and its direction corresponds to that of the stress. A distorted shape indicates a certain degree of anisotropy. For example, the directional dependence of the Young's modulus and linear compressibility for an orthorhombic crystal are given by[20].

$$E = \left[l_1^4 s_{11} + 2l_1^2 l_2^2 s_{12} + 2xl_1^2 l_3^2 s_{12} + l_2^4 s_{22} + 2l_2^2 l_3^2 s_{33} + l_3^4 s_{33} + l_2^2 l_3^2 s_{44} + l_1^2 l_3^2 s_{55} + l_1^2 l_2^2 s_{66} \right]^{-1} \qquad \text{(II.36)}$$

$$\beta = (s_{11} + s_{12} + s_{13})l_1^2 + (s_{12} + s_{22} + s_{23})l_2^2 + (s_{13} + s_{23} + s_{33})l_3^2 \qquad \text{(II.37)}$$

References

[1] L.H. Thomas, The calculation of atomic fields, Mathematical Proceedings of the Cambridge Philosophical Society, Cambridge University Press, 1927, pp. 542-548.
[2] E. Fermi, Eine statistische Methode zur Bestimmung einiger Eigenschaften des Atoms und ihre Anwendung auf die Theorie des periodischen Systems der Elemente, Zeitschrift für Physik 48 (1928) 73-79.
[3] E. Schrödinger, An undulatory theory of the mechanics of atoms and molecules, Physical review 28 (1926) 1049.
[4] P. Hohenberg, W. Kohn, Inhomogeneous electron gas, Physical review 136 (1964) B864.
[5] D. Ceperley, DM Ceperley and BJ Alder, Phys. Rev. Lett. 45, 566 (1980), Phys. Rev. Lett. 45 (1980) 566.
[6] A.D. Becke, Density-functional exchange-energy approximation with correct asymptotic behavior, Physical review A 38 (1988) 3098-3100.
[7] J.P. Perdew, Unified theory of exchange and correlation beyond the local density approximation, Electronic structure of solids' 91 11 (1991).
[8] J.P. Perdew, K. Burke, M. Ernzerhof, Generalized gradient approximation made simple, Physical review letters 77 (1996) 3865.
[9] B. Hammer, L.B. Hansen, J.K. Nørskov, Improved adsorption energetics within density-functional theory using revised Perdew-Burke-Ernzerhof functionals, Physical Review B 59 (1999) 7413.
[10] R. Wahl, D. Vogtenhuber, G. Kresse, SrTiO 3 and BaTiO 3 revisited using the projector augmented wave method: Performance of hybrid and semilocal functionals, Physical Review B 78 (2008) 104116.
[11] D. Khadidja, Propriétés électroniques et élastiques des semiconducteurs anorganiques, Université Ferhat Abbas de Sétif 1, 2012.
[12] N.W. Ashcroft, N. Mermin, Solid state, Physics (New York: Holt, Rinehart and Winston) (1976) 131-151,561.
[13] M. Sigrist, Solid State Theory, Institutes fl • ur Theoretische Physik HIT K23.8 (2014).
[14] G. Makov, R. Shah, M.C. Payne, Periodic boundary conditions in ab initio calculations. II. Brillouin-zone sampling for aperiodic systems, Phys Rev B Condens Matter 53 (1996) 15513-15517.
[15] M. Segall, P.J. Lindan, M.a. Probert, C. Pickard, P.J. Hasnip, S. Clark, M. Payne, First-principles simulation: ideas, illustrations and the CASTEP code, Journal of Physics: Condensed Matter 14 (2002) 2717.
[16] M.C. Payne, M.P. Teter, D.C. Allan, T. Arias, a.J. Joannopoulos, Iterative minimization techniques for ab initio total-energy calculations: molecular dynamics and conjugate gradients, Reviews of modern physics 64 (1992) 1045.
[17] H.J. Monkhorst, J.D. Pack, Special points for Brillouin-zone integrations, Physical review B 13 (1976) 5188.
[18] R. Hill, The elastic behaviour of a crystalline aggregate, Proceedings of the Physical Society. Section A 65 (1952) 349.
[19] O.L. Anderson, A simplified method for calculating the Debye temperature from elastic constants, Journal of Physics and Chemistry of Solids 24 (1963) 909-917.
[20] C.M. Kube, Elastic anisotropy of crystals, Journal of Applied Physics (2016).

Chapter III

Results and discussion

Chapter III: Results and discussion

III.1 Introduction

In this chapter, we will present the results for the optimized structural parameters and the predicted elastic and electronic properties for the ternary alkali metal antimonides A_2MP (*A=Na, K* and *M=Cu, Ag*) namely, *Na_2AuSb, Na_2AgSb and K_2AuSb*.

III.2 Calculation details

All calculations conducted in the present work were performed using CASTEP code based on the pseudo-potential and plane waves schemes (PP-PW) of DFT theory. We used Generalized Gradient Approximation (GGA) as parameterized by Perdew-Burk-Ernzerhof for solids "PBEsol".[1] Electron-ionic interactions were treated by Vendebilt ultra-soft pseudo-potentials[2]. Valence states were modelled by ($2s^2 2p^6 3s^1$) for Na, ($3s^2 3p^6 4s^1$) for K, ($5d^{10} 6s^1$) for Au, ($4d^{10} 5s^1$) for Ag and ($5s^2 5p^3$) for Sb. In a DFT calculation, the physical properties of a system are functional of the electron density of the ground state. This density is the one that minimizes the total energy of the system. It is therefore imperative to express this energy with the greatest possible precision. In order to ensure convergence of the computed structures and energetics, the parameters that affect the calculation accuracy were selected after performing careful convergence tests. The self-consistent loop was iterated until the total energy difference of the system between the consecutive iterating steps becomes less than 10^{-6} eV/atom. First, the Cut-off energy (**E_{cut}**) convergence study has been performed, than convergence with respect to Brillouin zone sampling has been conducted, the results are presented in the next section.

III.3 Convergence study

In practice, one must always test the convergence of the results with respect to the cut-off energy and with respect to the sampling grid of the of Brillouin zone. Usually, to obtain accurate values of the kinetic energy cut-off and the number of K-points ensuring the convergence of the total energy of the system with good accuracy, one varies the energy (E_{cut}) ranging from 200 to 1000 eV. For each of these values, we calculate the total energy and we plot the variation of the total energy curve as function energy cut-offs**.** The total energy is converged when the maximum relative variation ($\Delta E / E_F$) is stable within 10^{-6}.

In periodic solids, to get an accurate representation of the ground state density, the number of mono electronic ψ_{nk} orbitals in the plane waves basis set must be large. In practice calculations must be realized within a finite number of *K* points. Therefore, after setting the value of E_{cut}, we

proceed to sampling the Brillouin zone (BZ). We follow the same convergence procedure as the previous one.

The *K*-point sampling girds are varied from *(2x2x2)* to *(9x9x9)* for all cases. For each of these values, we calculate the total energy and we plot the curve of variation of the total energy according to the values of the number of *K*-points.

As shown on figure III-1 and figure III-2, it is obvious that good convergence is achieved for E_{cut}=700 eV and 7x7x7 K-point sampling gird in all three cases. Till now, all calculations will be performed on a plane wave basis set with a cut-off energy of 700 eV and a satisfactory 7x7x7 sampling gird of the Brillouin zone. For the sake of clarity, only calculations details for Na_2AuSb are reported in table III.1 and table III.2**.**

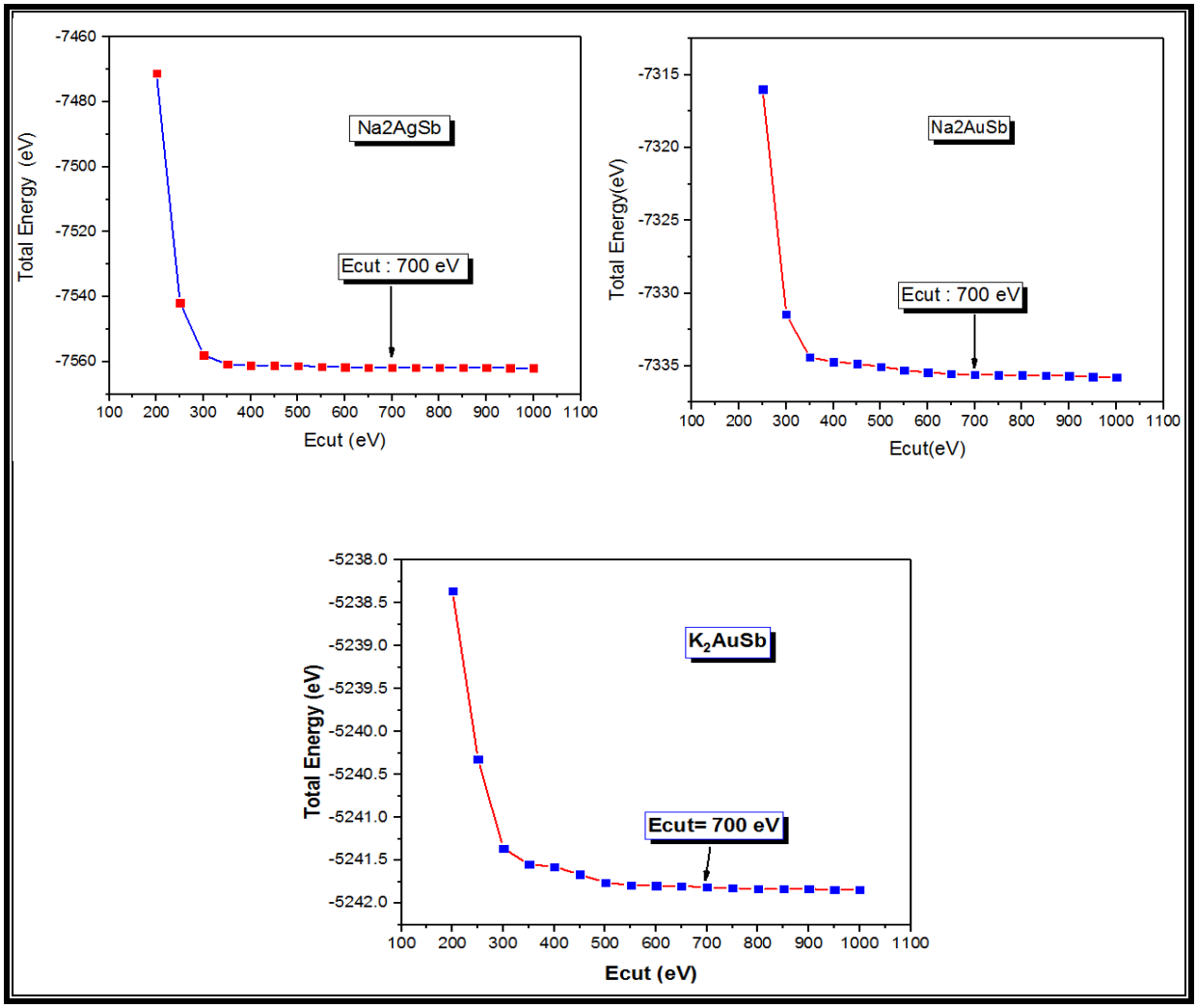

Figure III.1: *Convergence of the total energy as a function of E_{cut} for compounds (Na_2AuSb, Na_2AgSb and K_2AuSb).*

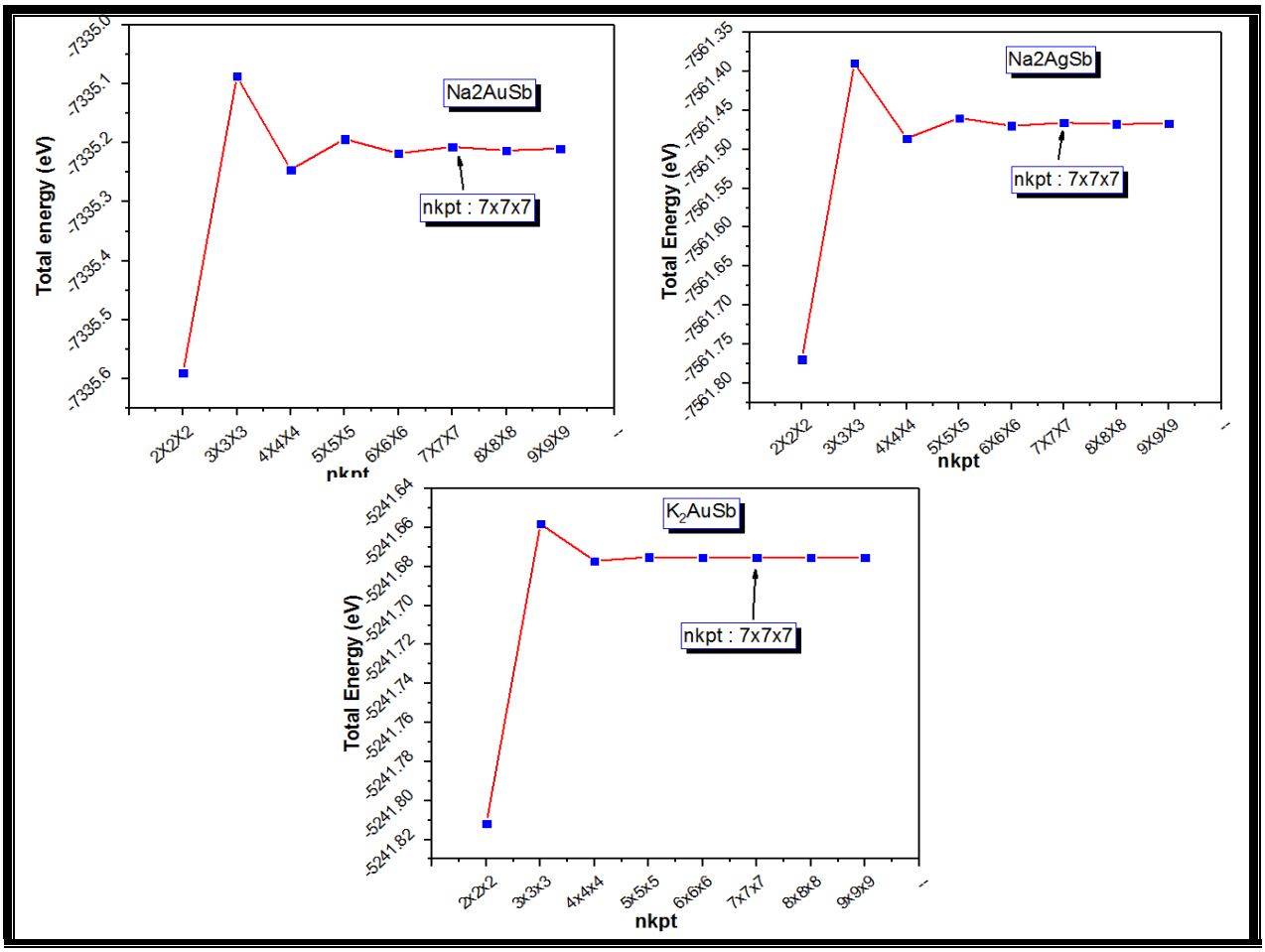

***Figure III.2**: Convergence of the total energy as a function of nkpt for compounds (Na2AuSb, Na_2AgSb and K2AuSb).*

***Table III.1** : Convergence total energy functional of Ecut for Na_2AgSb compounds(64 k-point).*

Na_2AgSb		
Ecut (eV)	***Total Energy (eV)***	$\Delta E / E_F$
200	-7471.12352	-0.011989674
250	-7541.83246	-0.00263885
300	-7557.9277	-0.000510353
350	-7560.80441	-0.000129926
400	-7561.11569	-8.87608E-05
450	-7561.14742	-8.45647E-05
500	-7561.27775	-6.73293E-05
550	-7561.46719	-4.2277E-05
600	-7561.63177	-2.05123E-05
650	-7561.72924	-2.27988E-06
700	**-7561.76964**	**-2.27988E-06**
750	-7561.77935	-9.95796E-07
800	-7561.78688	0

Table III.2: *Convergence total energy functional of k points ,for Na_2AgSb compounds (Ecut=700eV).*

K-points	*Total Energy (eV)*	$\Delta E / E_F$
2x2x2	-7561.76964	4.00646E-05
3x3x3	-7561.389242	-1.02429E-05
4x4x4	-7561.485836	2.53157E-06
5x5x5	-7561.459572	-9.4185E-07
6x6x6	-7561.4697	3.97579E-07
7x7x7	**-7561.46573**	**-1.27451E-07**
8x8x8	-7561.467468	1.02397E-07
9x9x9	-7561.466693	0

III.4 Equilibrium geometry and structural parameters

We first started to examine whether the selected calculation parameters reproduce the experimental equilibrium geometry for *Na_2AuSb , Na_2AgSb ,K_2AuSb***.** In CASTEP, the structure relaxation procedure is realized self consistently by allowing unit cell parameters and atomic coordinates to be relaxed. The Broyden-Fletcher-Goldfarb-Shanno (BFGS) algorithm [3] allows a rapid determination of the ground state geometry. In the process of minimization, a given structure is considered as the ground state geometry if the following criteria are fulfilled:

- Tolerance in energy: 10^{-6} eV/atom.
- Max force: 0.005 eV/Å.
- Max stress: 0.01 GPa.
- Max displacement: $5.0x10^{-4}$Å.

For the subsequent optimizations, the initial experimental equilibrium geometries were taken from Ref. [4] for *Na_2AuSb*, Ref. [5] for *Na_2AgSb* and Ref. [4] for *K_2AuSb*. The obtained results are summarized in Table III-3, along with the available experimental data for comparison.

Form the data in Tables III.3, III.-4 and III.-5, it can be clearly seen that the optimized equilibrium structural parameters, atomic coordinates and selected interatomic distances are in excellent agreement with the available experimental values [4, 5]. For instance, the maximum deviation between herein calculated lattice parameters and the experimental results is within 1.*62* %, while the maximum deviation between the optimized atomic coordinates and the experimental values is 1.77% (see table III.5). The excellent agreement between the calculated results and their experimental counterpart demonstrates the reliability of the computational methodology adapted here, and gives confidence on the subsequent results for elastic and electronic properties. As can

be expected, with increasing the alkali-metal and the noble metal atomic radius, going down the periodic table column from *Na* to *K* and from *Ag* to *Au* , the unit cell volume is found to be increased.

***Table III.3**: The cell parameters, the corresponding volume and density of compounds.*

		***a* (Å)**	***b* (Å)**	***c* (Å)**	**V (Å^3)**	$\rho(g/cm^3)$
	Present	10.411	7.819	6.411	521.854	5,052
K$_2$AuSb	*Exp.*	10.450	7.857	6.501	533.779	4,939
	***d* (%)**	0.37	0.48	1.38	2.23	2.29
	Present	9.305	7.473	5.842	406.223	5,963
Na$_2$AuSb	*Exp.*	9.279	7.562	5.841	409.850	5,910
	***d* (%)**	0.28	1.17	0.017	0.88	0.90
	Present	9.270	7.775	5.731	413.081	4,432
Na$_2$AgSb	Exp.	9.292	7.903	5.773	423.938	4,318
	***d* (%)**	0.24	1.62	0.73	2.56	2.64

***Table III.4**: Atomic positions of (Na$_2$AuSb, Na$_2$AgSb, K$_2$AuSb).*

Compounds	**Atoms**	***x***		***y***		***z***	
		Present	***Exp***	***Present***	***Exp***	***Present***	***Exp***
	K	0.67113	0.67030	0.82988	0.83670	0.25000	0.25000
K$_2$AuSb	*Au*	0.50000	0.50000	0.50000	0.50000	0.00000	0.00000
	Sb	0.50000	0.50000	0.22555	0.23555	0.25000	0.25000
	Na	0.32052	0.32250	0.33025	0.33890	0.25000	0.25000
Na$_2$AuSb	*Au*	0.50000	0.50000	0.00000	0.00000	0.00000	0.00000
	Sb	0.00000	0.00000	0.19664	0.20760	0.25000	0.25000
	Na	0.32132	0.32290	0.34543	0.35230	0.25000	0.25000
Na$_2$AgSb	*Ag*	0.50000	0.50000	0.00000	0.00000	0.00000	0.00000
	Sb	0.00000	0.00000	0.20526	0.21270	0.25000	0.25000

***Table III.5:** Distances interatomic (A°) for Na$_2$AuSb, Na$_2$AgSb and K$_2$AuSb compounds*

A$_2$XSb	***A – Sb***		***A – X***		***Sb – X***		***X – X***	
	present	***Exp***	***present***	***Exp***	***present***	***Exp***	***present***	***Exp***
K$_2$AuSb	3.69277	3.79072	3.52072	3.71109	2.67828	2.64635	3.20535	3.25000
Na$_2$AuSb	3.14505	3.37130	3.31858	3.54561	2.69679	2.64980	2.92100	2.92050
Na$_2$AgSb	3.33326	3.36211	3.46550	3.52815	2.70266	2.69041	2.86560	2.88650

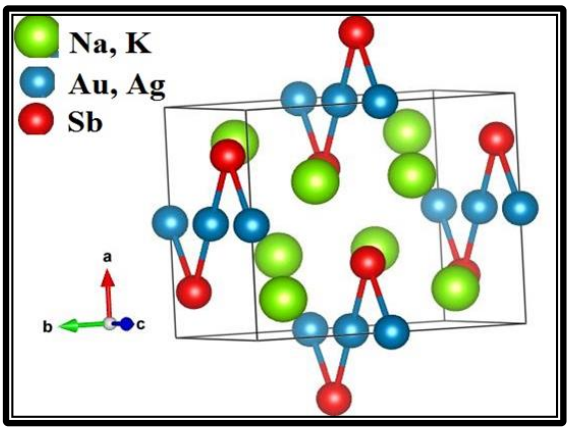

***Figure III-3**: The orthorhombic unit cell of the compounds (space group Cmcm).*

III.5 Electronic properties

The calculations of the electronic properties provide significant information for understanding the physical properties and bonding nature of materials. Therefore the study of bonding characteristics of Na_2AuSb , Na_2AgSb ,K_2AuSb is so important. In this case the study of the electronic band structure and the density of states (DOS) play the most significant task. In order to get a deep insight about the bonding nature of this compound, the total density of states (TDOS) and the partial density of states (PDOS) have been also calculated.

III.5.1 Structure of the energy bands

The energy bands give the possible energies of an electron as a function of the wave vector. These bands are thus represented in the reciprocal space, and for simplicity, only the directions between the high symmetries points in the first Brillouin zone are treated. Figure III-4 gives a comparison between the structure of the energy bands of the three materials (Na_2AuSb, Na_2AgSb, K_2AuSb).

The investigated compounds show the same features and the bands are large dispersing around the Fermi level. As can be seen from Figure III-4, all three materials have narrow band gaps of about 0.896 eV, 0.464 eV and 0.183 eV for K_2AuSb, Na_2AgSb and Na_2AuSb recpectivly, revealing their semiconducting nature. The band gaps are found to be indirect as the maximum of the valence band (VB) lies at the Y point and the minimum of the conduction band (CB) occurs at the G point. The flatness of the valence bands in the energy rage -6 eV to -3eV, implies that d-électrons are playing important role in the bonding figure.

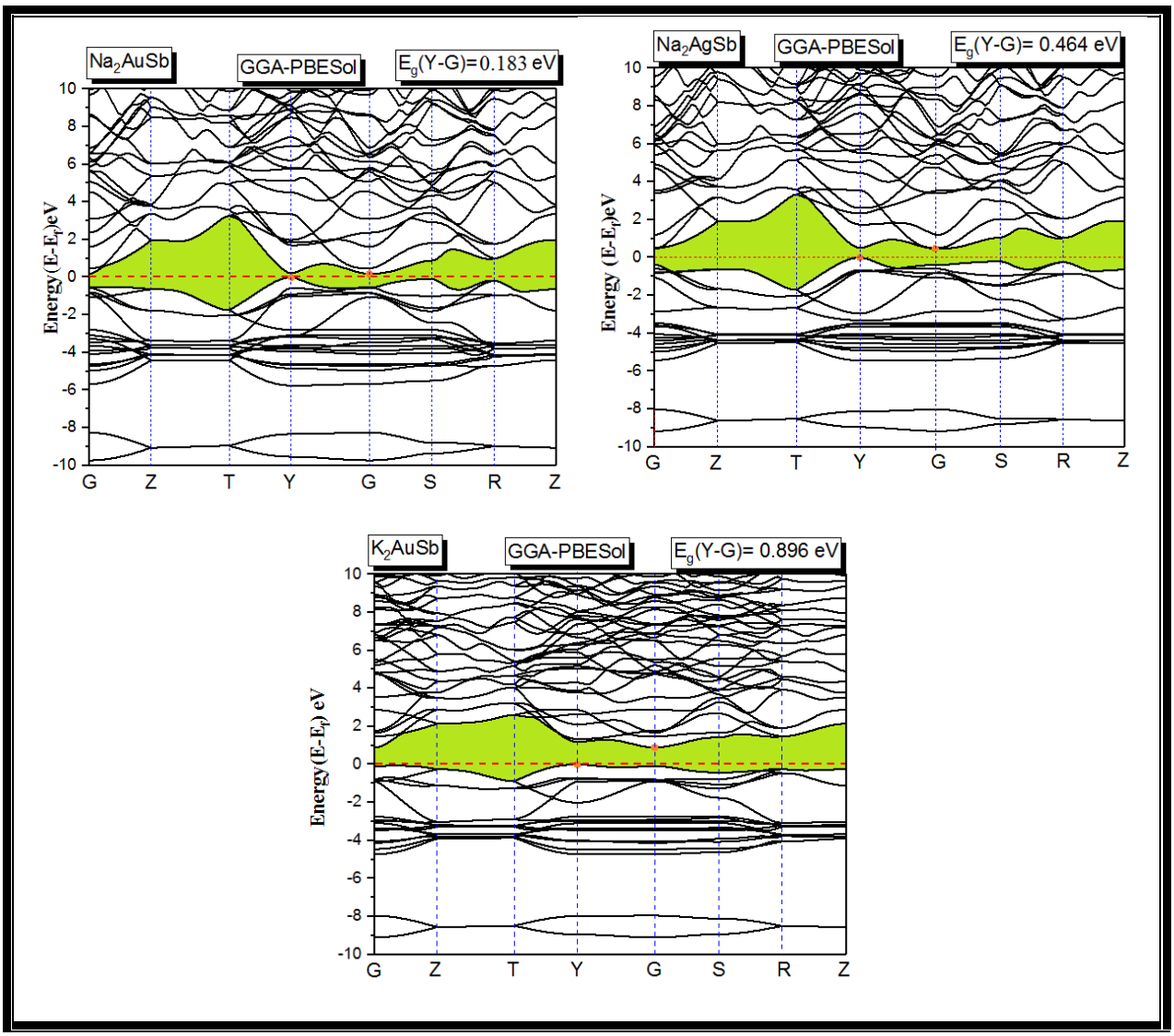

Figure III.4: *Energy band structures of Na_2AuSb;Na_2AgSb;,K_2AuSb, calculated by GGA PBESol.*

III.5.2 Density of states

The density of states (DOS) is an important physical quantity to understand the electronic states in a material and their influence on its physical properties. Most of the electronic transport properties are determined on the basis of knowledge of the density of states. It also allows to know the nature of the chemical bonds in a material, and therefore the charge transfer between the orbitals and the atoms. Are shown in figure III-5, the density of stat curves for the considered materials. One can clearly observe the existence of three valleys in the valence region (BV1, BV2, BV3). The first valley (BV1) is located between [-9eV-8eV] and originated predominately from *Sb*-s and the transition metal p and d sates. The second valley (BV2) which is stretched between [-6eV-3eV] for the sodium based compounds, namely (*Na_2AuSb, Na_2AgSb*) and [-5eV-3eV] for

the potassium based compound *K_2AuS*, is completely dominated by the transition metal d orbitals with a small contribution from transition metal p and *Sb*-p states. The third valley (BV3) which spreads between [-3eV 0eV], is mainly due to the Sb-p orbitals. The bottom of the conduction band is made up of an admixture of s and p orbitals of the Sb, the transition metal and the alkali metal atoms, while the top of the conduction band is dominated by the alkali metal p orbitals. Form the DOS curves, it is obvious that the alkali metal atoms do not contribute significantly in the valence band region, but have key role in the conduction band, and this suggests that the alkali metal atoms tend to establish ionic bonds with their nearest neighbors.

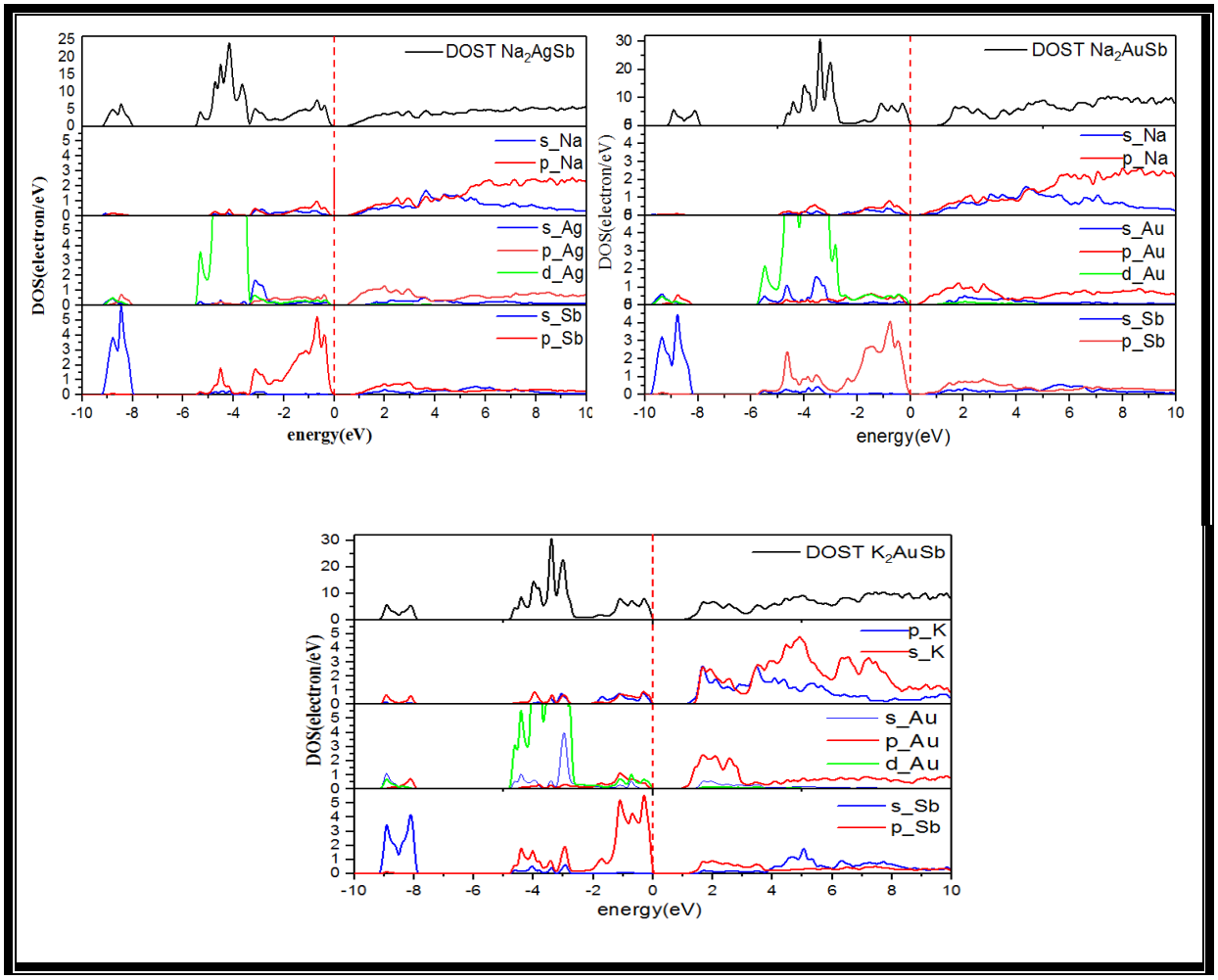

***Figure III.5**: Total and partial density of states for Na_2AuSb; Na_2AgSb;K_2AuSb compounds.*

III.5.3 Bonding picture

To further understand interatomic bonding behaviors of the considered crystals, the calculated atomic populations, bond length and atomic charges via the Mulliken population analysis are listed in Table III.6. It is found that for all three materials, the charge transfers from the alkali metal atoms to the Sb and the transition metal atoms. The transfer numbers are found to

be: 0.54 for *K* and -0.94, -0.14 for *Au* and *Sb* in case of K_2AuSb; 0.60 for *Na* and -0.68, -0.51 for *Au* and *Sb* in case of Na_2AuSb, 0.50 for *Na* and -0.55, -0.45 for *Ag* and *Sb* in case of Na_2AgSb. This propose valence stats of $(K^{+0.54})_2Au^{-0.94}Sb^{-0.14}$, $(Na^{+0.60})_2Au^{-0.68}Sb^{-0.51}$ and $(Na^{0.50})_2Ag^{-0.55}Sb^{-0.45}$. The values of the Mulliken transfer numbers are representative of the ionic and covalent bonding in the considered materials. To get more insight into the bonding character of the ternary alkali metal antimonied, band populations have been also calculated. Generally, a high value of positive population indicates a high degree of covalency in the bond, while low values of band population indicate ionic bonding character (see figure III.6). Results depicted in table III.6 give evidence for a low covalent bonding between *Au* atoms and *Sb* atoms for Na_2AuSb and K_2AuSb, and a somewhat weak ionic bounding between *Ag* and *Sb* atoms for Na_2AgSb in the zigzag chains along the c-axis.

***Table III.6**: Mulliken atomic population and Bond lengths of Zigzag chain for Na_2AuSb; Na_2AgSb and K_2AuSb compounds..*

		s (e)	*p (e)*	*d (e)*	*Total (e)*	*Charge (e)*
	K	2.28	6.19	-	8.46	0.54
K_2AuSb	Au	1.32	0.87	9.75	11.94	-0.94
	Sb	1.25	3.89	-	5.14	-0.14
	Na	2.13	6.28	-	8.40	0.60
Na_2AuSb	Au	1.07	0.91	9.70	11.68	-0.68
	Sb	1.87	3.64	-	5.51	-0.51
	Na	2.19	6.31	-	8.50	0.50
Na_2AgSb	Ag	0.84	0.90	9.81	11.55	-0.55
	Sb	1.70	3.75	-	5.45	-0.45

	Bond	*Population*	*Length (A°)*
K_2AuSb	*Sb – Au*	0.53	2.67828
Na_2AuSb	*Sb – Au*	0.63	2.69679
Na_2AgSb	*Sb – Ag*	0.37	2.70266

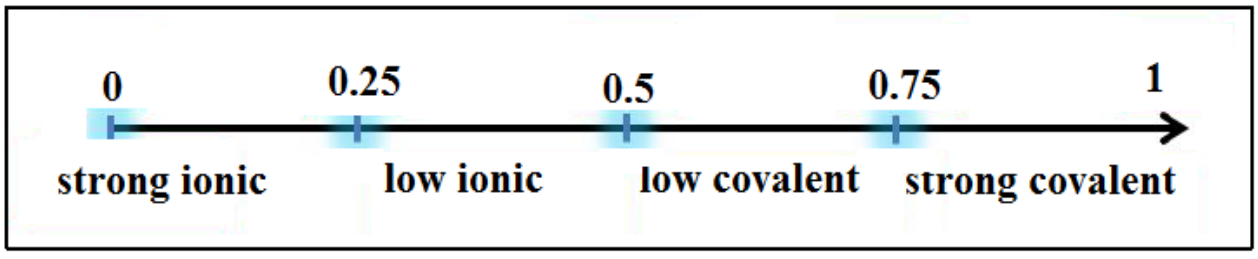

***Figure III.6:** Classification of the nature of the bonds according to Mulliken population analysis.*

In order to visualize the nature of the bonding character and to explain the charge transfer in Na_2AuSb, Na_2AgSb *and* K_2AuSb we calculate the valence charge density. Figure III.7 shows the

calculated valence charge density in the (1 0 0), clearly revealing the covalent bounding between the transition metal atoms and the Sb atoms in the zigzag chains along the c- axis. Moreover, a clear bonding interaction can be seen between the transition metals atoms along the c- axis. This trend has been also reported for other compounds containing Au toms and containing the same crystallographic features[12].

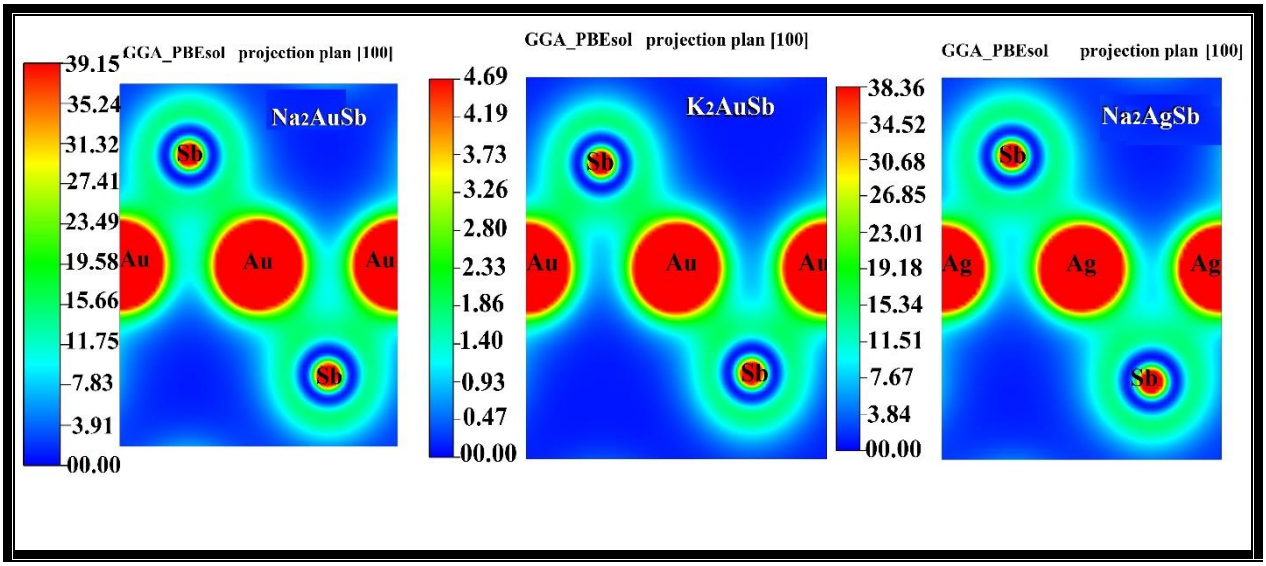

***Figure III.7**: The bonding charge density plots in the (100) plane of the Na_2AuSb and Na_2AgSb; K_2AuSb.*

III.6 Elastic properties

The elasticity treats the relationship between strains and stresses of a solid under the influence of external forces. It is related to several fundamental solid-state phenomena and physical properties such as mechanical stability, phonon frequency, sound velocity, Debye temperature, specific heat, thermal expansion, melting point … etc.

III.6.1 Tensor of elastic stiffness constants (C_{ij})

Using the above-determined equilibrium geometries, the complete set of elastic stiffness constants (C_{ij}) were calculated using the stress–strain method as described in Ref [6]. Different strain patterns are applied to the initial equilibrium geometry and the corresponding stress is calculated. For an orthorhombic crystal, three unique symmetry related strain patterns -the first with non-zero ε_{xx} and ε_{yz},the second with non zero ε_{yy} and ε_{xz}, the third ε_{zz} and ε_{xy} - are sufficient to cause all nine elastic stiffness constants, namely; $C_{11}, C_{22}, C_{33}, C_{44}, C_{55}, C_{66}, C_{12}, C_{13}$. To stay within elastic domain and to avoid computational noise which maybe significant for closely similar structures, four stain amplitudes were used with a maximum deformation of 0.3% . The obtained results are summarized in table III-7.

***Table III.7**: Elastic stiffness constants (in GPa) calculated for our compounds.*

	C_{11}	C_{22}	C_{33}	C_{44}	C_{55}	C_{66}	C_{12}	C_{13}	C_{23}
K_2AuSb	41.59	35.45	24.20	19.06	7.74	7.46	6.52	5.20	13.40
Na_2AuSb	54.60	64.81	59.17	24.73	10.64	11.24	10.11	6.81	31.05
Na_2AgSb	48.85	47.88	59.24	20.66	11.53	9.43	7.60	5.75	24.64

The three stiffness constants C_{11}, C_{22} and C_{33} represent resistance to unidirectional compression along the main directions [100], [010] and [001], respectively. The other six constants: $C_{44}, C_{55}, C_{66}, C_{12}, C_{13}$,and C_{23} are a measure of resistance to shear stresses. As one can see from table III-6, the values for C_{11}, C_{22} and C_{33} are larger than those for C_{44}, C_{55}, C_{66}, C_{12}, C_{13} , C_{23} demonstrating that the present materials are more resistant to uniaxial deformations than to shear deformations.

III.6.2 Mechanical stability

For a crystal to be mechanically stable, the strain energy must be positive. This means, for an orthorhombic crystal that the elastic stiffness constants should fulfill the following born stability criteria [7]:

$$\begin{cases} C_{ij} > 0 \ ; \ (i, j = 1...6) \\ (C_{11} + C_{22} - 2C_{12}) > 0 \ ; \\ (C_{11} + C_{33} - 2C_{13}) > 0 \ ; \\ (C_{22} + C_{33} - 2C_{23}) > 0 \ ; \\ (C_{11} + C_{22} + C_{33} + 2C_{12} + 2C_{13} + 2C_{23} > 0 \end{cases} \quad \text{(III-1)}$$

Further analysis of the numerical estimate of the nine elastic stiffness constants show that all the aforementioned stability criteria are verified, suggesting mechanical stability of the three compounds.

III.6.3 Polycrystalline elastic moduli

The calculation of the latter elastic constants makes it possible to get accurate numerical estimations of other polycrystalline elastic moduli such as Young's modulus, shear modulus and Poisson's coefficient (see table II-3). The obtained results following the Voigt-Reuss-Hill approximation for *Na_2AuSb*, *Na_2AgSb* and *K_2AuSb* are summarized in table III-8. In this approach, the Voigt (denoted V in index) and Reuss (denoted R) moduli are the lower and upper bounds of *B* and *G*, while Hill (denoted H) gives the means between the two limits.

Actually, all three materials are characterized by low values of bulk modulus (*B*), suggesting that these materials are soft and easily compressible. The somewhat lower values of *G* indicates weaker ability to withstand shear strain, implying that the parameters limiting mechanical stability of these materials is the shear modulus *G*. Furthermore, as can be seen from table III-8, the values of Young's moduli *E* of all three materials are small. This confirms that these materials have weak stiffness. A weak hardness can be expected from the aforementioned results and this is confirmed by the low values of the numerical estimate of Vickers hardeness from Chens's model [8].

According to Pugh's criterion [9], (*B/G*) of polycrystalline phases could be used to predicate the brittle (*B/G* < 1.75) and ductile (*B/G* > 1.75) behaviors. In light of the Pugh's viewpoint, *K_2AuSb* and *Na_2AgSb* must be classified as fragile material ($B_H / G_H \prec 1.75$), while *Na_2AuSb* must be classified as ductile material ($B_H / G_H \succ 1.75$).

Table III.8: *Calculated bulk modulus (B, in GPa), shear modulus (G, in GPa), Young's modulus (E, in GPa), Hardness (H, in GPa), B/G ratio and Poisson ratio υ. The subscripts V, R and H stand to Voigt, Reuss and Hill approximations, respectively.*

	K_2AuSb	***Na_2AuSb***	***Na_2AgSb***
B_V	16.83	30.50	25.77
B_R	16.22	29.16	24.91
G_V	11.93	18.03	16.19
G_R	9.95	15.36	14.15
B_H	16.53	29.83	25.34
G_H	10.94	16.70	15.17
B/G	1.51	1.78	1.67
E	26.89	42.22	37.93
υ	0.23	0.26	0.25
H_V	2.70	2.87	2.92

Many phenomena in the deformation of elastic materials depend on the Poisson's ratio. The simplest is that a material with a negative Poisson's ratio will get fatter in cross section when stretched and thinner when compressed. As the value of Poisson's ratio approaches 0.5, as with the rubber like materials, the material easily undergoes shear deformations but resists volumetric deformation and becomes incompressible [10]. The typical υ value is 0.1 for brittle covalent materials, 0.33 for ductile metallic materials and 0.25 for ionic materials, respectively. For *K_2AuSb*, Poisson's ratio is smaller than 0.25, so we can classify this material as brittle, while for *Na_2AuSb* Poisson's is greater than 0.25 suggesting that this compound should be classified as ductile. These results are in good agreement with results obtained from analysis of B/G ratio. Moreover, in all three cases, Poisson's ratio is close or equal to 0.25, suggesting that more ionic contribution to interatomic bonding should be considered.

III.6.4 Debye Temperature

Debye temperature θ_D is a suitable physical parameter to describe some the phenomena of solid-state physics, which is associated with lattice vibration, thermal conductivity, melting temperature and specific heat. It reflects also strength of chemical bonding in crystalline materials. We may calculate the Debye temperature of *Na_2AuSb*, *Na_2AgSb* and *K_2AuSb* compounds using average sound velocity V_m, the longitudinal propagation velocities v_l, transverse v_t as given by the equations (II:28;29; 30; 31), in chapter II. The obtained results are presented in Table III-9. As can be seen from this table, all three materials are characterized by low Debye temperature. The order of the calculated θ_D for our compounds is $\theta_D(\boldsymbol{K_2AuSb}) < \theta_D(\boldsymbol{Na_2AuSb}) < \theta_D(\boldsymbol{Na_2AgSb})$.

Since, at lower temperatures, phononic excitations are solely determined by the acoustic modes, the lower Debye temperature suggest lower phonon frequency. As a rule of thumb, a lower Debye temperature implies lower thermal conductivity and melting temperature which are almost associated to weakest chemical bonding and stiffness in corresponding crystal structure.

Table III.9*: Debye temperature, density and velocity of wave propagation longitudinal, transverse and medium*

	$\rho(g/cm^3)$	$v_l(m/s)$	$v_t(m/s)$	$v_m(m/s)$	$\theta_D(K)$
K_2AuSb	5,052	2482	1742	1890	176
Na_2AuSb	5,963	2956	1673	1861	188
Na_2AgSb	4,432	3206	1850	2054	207

III.6.5 Anisotropy of elastic moduli

Crystal anisotropy decides atomic arrangements to follow a certain direction. It is very important to investigate anisotropic behaviors in crystal physics as well as in engineering science. The degree of anisotropy of a materials is measured by the relationship (II.32) which define the universal anisotropy index[11]. A value of zero indicates a perfect isotropic behavior of the elastic properties of marital, whereas a higher value indicates a degree of elastic anisotropy. In this work, the calculated universal anisotropic indexes A^U in all three cases are greater than zero -(A^U = 1.033; 0.915; 0.755) for K_2AuSb; Na_2AuSb and Na_2AgSb respectively- the large deviation from zero refer to a high anisotropic mechanical properties.

A more straightforward way to reveal elastic anisotropy is based on a three-dimensional surface plot of the directional dependence of elastic moduli (see chapter 2). Figure III-8 shows that, all three materials have anisotropic behavior of the Young's modulus since deviation from a perfect sphere is clear, this result agree well with results from analysis of universal elastic anisotropy indexes.

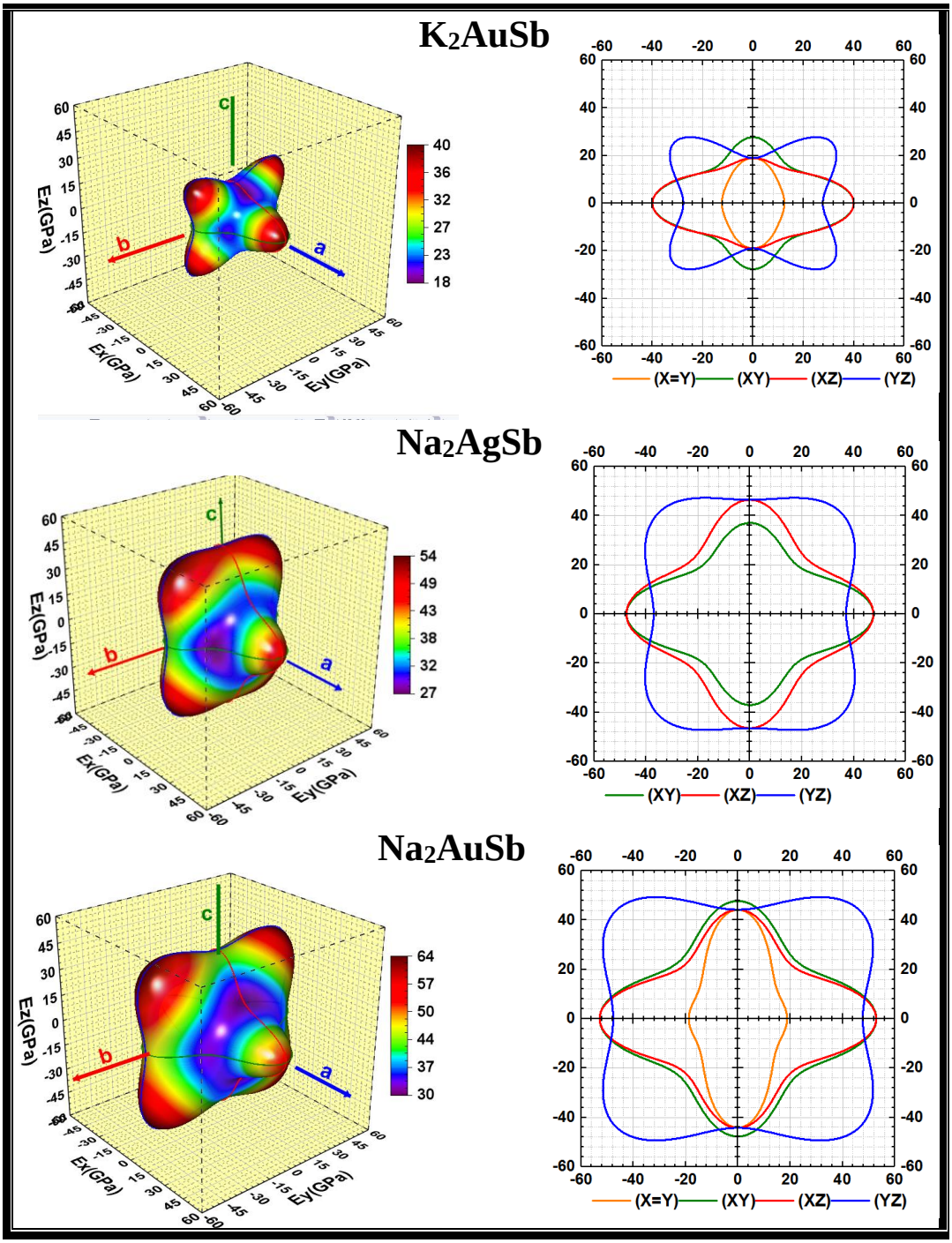

***Figure III.8**: Anisotropy of Young's modulus in Na_2AuSb; Na_2AgSb and K_2AuSb compounds.*

Cross-sections of the 3D-surfaces quoted in the right panels of Figure III.8, show that the maximum values of the Young's modulus occur when the stress is applied along the a-crystallographic axe and along the bisector direction in the (bc) coordinate plane, while the minimum values are realized when the stress is applied along the bisector direction in the (ab) and (ac) coordinate planes.

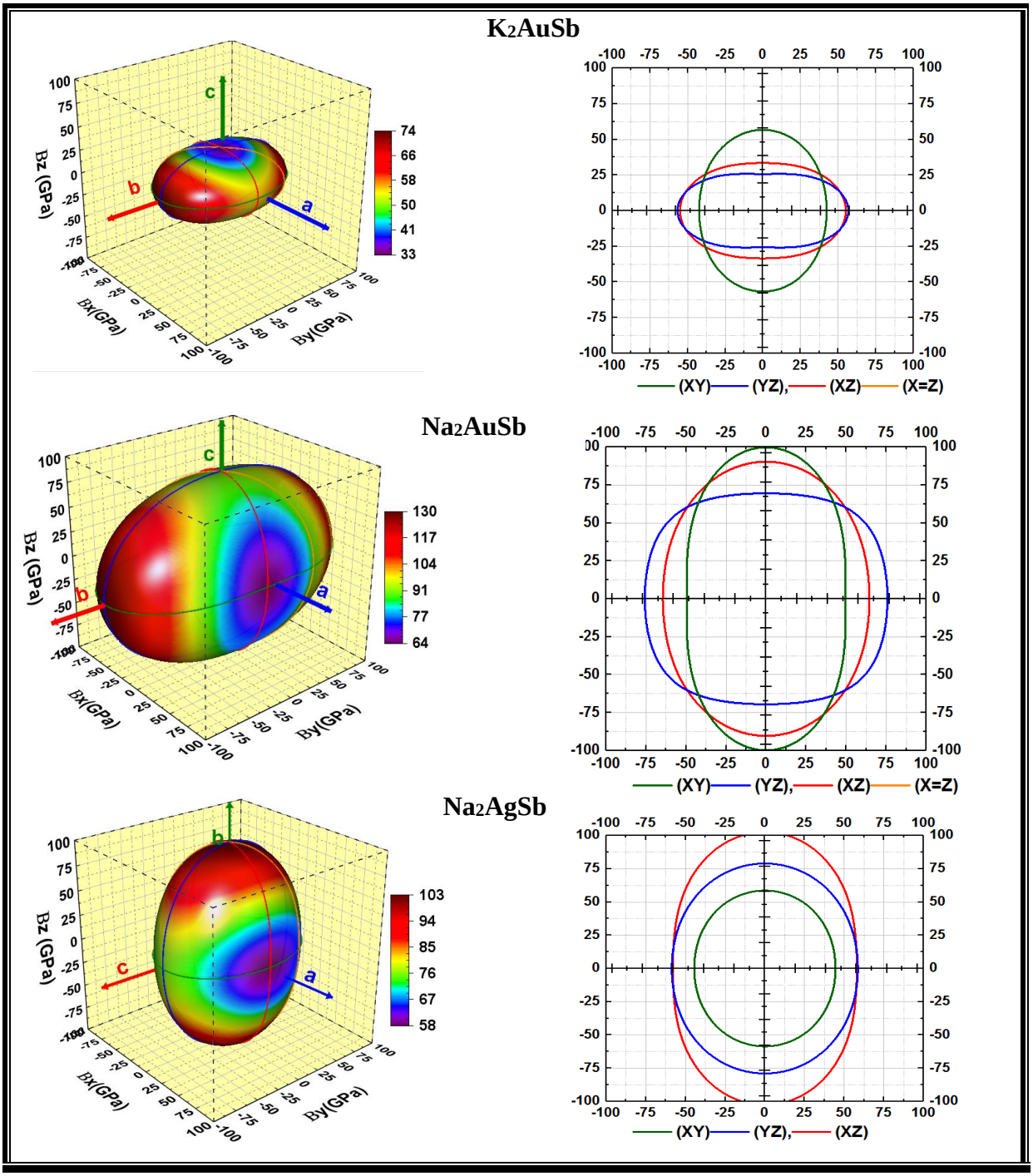

***Figure III.9**: Anisotropy of bulk modulus for (Na_2AuSb;Na_2AgSb and K_2AuSb) compounds.*

According the figure III-9, we can say that the bulk modulus is anisotropic for the three materials. However, anisotropy of bulk modulus is less discernable than anisotropy of Young's modulus, this suggests that anisotropy in the present cases arises predominately from anisotropy of shear modulus. Interestingly, cross-sections of the 3D-surfaces quoted in the right panels of Figure III.9 give evidence that the *b*- axis is the most incompressible for all three materials, while

the a- axis is the most compressible in case of sodium based compounds (*Na2AuSb, Na2AgSb*) and c-axis is the most compressible in case of potassium based compound (K_2AuSb).

References

[1] J.P. Perdew, K. Burke, M. Ernzerhof, Generalized gradient approximation made simple, Physical review letters 77 (1996) 3865.

[2] A. Guechi, A. Merabet, M. Chegaar, A. Bouhemadou, N. Guechi, Pressure effect on the structural, elastic, electronic and optical properties of the Zintl phase KAsSn, first principles study, 2014.

[3] T.H.F.a.J. Almlof, pp. 9768-9774, , The Journal of Physical Chemistry vol. 96.

[4] C. Mues, H.-U. Schuster, Na2AuAs, Na2AuSb, K2AuSb-drei neue A2BX-Verbindungen mit BX-Kettenstruktur/Na2AuAs, Na2AuSb, K2AuSb-Three New A2BX Compounds with a BX Chain Structure, Zeitschrift für Naturforschung B 35 (1980) 1055-1058.

[5] H. Schuster, C. Mues, W. Jung, Darstellung und Kristallstruktur des Na2AgSb, Z. Naturforsch. 34b (1979) 354-355.

[6] R. Hill, The elastic behaviour of a crystalline aggregate, Proceedings of the Physical Society. Section A 65 (1952) 349.

[7] F. Mouhat, F.-X. Coudert, Necessary and sufficient elastic stability conditions in various crystal systems, Physical Review B 90 (2014) 224104.

[8] X.-Q. Chen, H. Niu, D. Li, Y. Li, Modeling hardness of polycrystalline materials and bulk metallic glasses, Intermetallics 19 (2011) 1275-1281.

[9] S.F. Pugh, XCII. Relations between the elastic moduli and the plastic properties of polycrystalline pure metals, The London, Edinburgh, and Dublin Philosophical Magazine and Journal of Science 45 (1954) 823-843.

[10] L. RS., Foam structures with a negative Poisson's ratio, Science

;235(4792):1038–40. (1987).

[11] C.M. Kube, Elastic anisotropy of crystals, Journal of Applied Physics (2016).

[12] S.J. Kim, G.J. Miller, J.D. Corbett, Zigzag chains of alternating atoms in A2AuBi (A= Na, K) and K2AuSb. Synthesis, structure, and bonding, Zeitschrift für anorganische und allgemeine Chemie 636 (2010) 67-73.

Conclusion

Conclusion

By a theoretical calculation carried out in the framework of the DFT and the pseudopotential - plane wave method, structural, elastic and electronic properties of the ternary alkali metal antimonied have been investigated. The semilocal GGA-PBESol functional was applied to describing all the aforementioned properties.

The main findings of this study are:

- The calculated structural parameters agree well with the available experimental data.
- The studied materials are mechanically stable and exhibit a noticeable elastic anisotropy, they are soft and easily compressible with rather weak stiffness and weak hardness.
- The studied materials are characterized by low Debye temperatures, suggesting low phonon frequency and lattice thermal conductivity. This is an important parameter for a material to be a good thermoelectric material.
- The calculated band structure using the GGA-PBESol functional reveal that the considered compounds are narrow band gap semiconductors with indirect band gaps ranging between 0.183 eV and 0.896 eV.
- Mulliken population analysis and charge transfer numbers give evidence for a low covalent bonding between Au and Sb atoms, and a somewhat weak ionic bonding between Ag and Sb atoms in the zigzag chains along the c- axis.
- The projected charge density in the (100) plane shows some bonding interaction between neighboring Au atoms along the zigzag chains.

It should be noted that Na_2AuSb, Na_2AgSb and K_2AuSb are known to be highly air sensitive like other Zintl compounds. In order to realize devices for technological applications, one needs to take special care by synthesizing them in a low-oxygen or vacuum environment.

ملخص

لمعرفة الخصائص البنيوية، المرونية، الإلكترونية للمركبات القطبية الثلاثية (K_2AuSb,Na_2AuSb,Na_2AgSb) قمنا بدراسة نظرية حول هذه المركبات و ذلك باستخدام برنامج CASTEP الذي يعتمد على نظرية الكثافة الدالية (DFT) ، من بين العديد من التقريبات لحساب طاقة التبادل و الترابط ، استعملنا تقريب التدرج المعمم (GGA-PBESol) . النتائج المتحصل عليها كانت متوافقة مع النتائج التجريبية، حيث بينت هذه الدراسة أن المركبات Na_2AgSb, K_2AuSb ذات طبيعة هشة أما بالنسبة Na_2Ausb ذو طبيعة لدِنةٍ (لينة) و غير مقاومه للإجهاد . الخصائص الإلكترونية أظهرت أن هذه المواد عبارة عن أشباه موصلات ذات فجوات طاقة غير مباشرة ومتفاوتة القيم. تحليل موليكان و توزيع الكثافة الشحنية بينت ان الروابط بين ذرة الأنتيمون (Sb) و ذرة الذهب(Au) تساهمية ضعيفة بالنسبة للمركبات K_2AuSb، Na_2AuSb و بين ذرة الأنتيمون (Sb) و ذرة الفضة أيونية ضعيفة في المركب Na_2AgSb.

كلمات مفتاحية: نظرية الكثافة الدالية, تقريب التدرج المعمم, الخصائص البنيوية ,الخصائص الإلكترونية, الخصائص المرونية,أشباه الموصلات, المركبات القطبية الثلاثية.

Abstract

For the structural, elastic, electronic properties of ternary polar intermetallic compounds (K_2AuSb, Na_2AuSb, Na_2AgSb). We have studied theoretically about these compounds using CASTEP code, which relies on DFT, among many of the approximations for calculate the energy of exchange and correlation, using the GGA-PBESol (GGA) approximation. The results obtained were consistent with the results experimental. The study showed that Na_2AgSb and K_2AuSb were brittle in nature and Na_2Ausb was soft, non-stress resistant, and electronic properties showed that these materials were indirect semiconductors and different values of the energy gap. Mulliken population analysis and distribution the density of the charge a, demonstrated that the bond between the antimony *(Sb)* and gold *(Au)* atoms is low covalent for K_2AuSb, Na_2Ausb and between the *(Sb)* antimony and silver atom (Ag) is low ionic bonding for Na_2AgSb.

***Key words*: DFT, GGA, Structural, electronic, elastic properties, semiconductor, triangular polar intermetallic compounds.**

Résumé

Pour les propriétés structurelles, élastiques, électroniques des composés intermétalliques polaires ternaire (K_2AuSb, Na_2AuSb, Na_2AgSb). Nous avons étudié théoriquement ces composés en utilisant le code CASTEP, qui repose sur la DFT, parmi de nombreuses approximations de l'énergie d'échange et de corrélation, en utilisant l'approximation GGA-PBESol (GGA). Les résultats obtenus étaient en accord avec les résultats expérimentaux. L'étude a montré que Na_2AgSb et $K2AuSb$ étaient de nature fragile et que Na_2Ausb était ductile, non résistant aux contraintes, et que les propriétés électroniques montraient que ces matériaux étaient des semi-conducteurs indirects et différentes valeurs de l'écart énergétique. Mulliken population analyse et distribution de la densité de la charge et la densité de stat, a montré que la liaison entre les atomes d'antimoine (*Sb*) et or (*Au*) est faible covalente pour K_2AuSb, Na_2Ausb et entre l'antimoine (*Sb*) et l'atome d'argent (*Ag*) est une faible liaison ionique pour Na_2AgSb.

***Mots clés* : DFT, GGA, propriétés structural, élastiques, électroniques, semi-conducteurs, intermétalliques polaires triangulaires.**